NMR Measurements with Narrow-band Probes

Soumyajit Mandal

Abstract

We carry out a thorough analysis of the challenges involved in making NMR measurements with the narrow-band front-end circuits (probes) used in low-frequency measurements. We derive simple circuit models of these probes and solve them analytically. We then describe how to create a combined model of the entire measurement by interfacing these circuit models to spin dynamics calculations. As one example of the possible applications, we embedded our model inside an optimization algorithm. This allowed us to derive phase-modulated RF pulses at Larmor frequencies of 250 kHz and 500 kHz that substantially increase the signal-to-noise ratio (SNR) of the measurement without increasing average power consumption.

Contents

Introduction

Nuclear magnetic resonance (NMR) is widely used in physics, analytical sciences, medical imaging, and geological prospecting. The NMR signal originates from the resonant irradiation and interaction of RF magnetic fields with nuclear spins in a static magnetic field. Traditionally, the experimental apparatus has employed a tuned and matched resonant circuit to achieve efficient transmission of the RF power for spin manipulation and significant voltage gain with out-of-band noise rejection. This technology was borrowed from radio and radar electronics and the resonant circuit typically consists of a metallic wire-wound coil (inductance L) and a tuning capacitor (capacitance C). The tuned resonant circuit acts as an analog filter at its resonance frequency $\omega_c \approx 1/\sqrt{LC}$ with a bandwidth of approximately ω_c/Q, where Q is the quality factor of the coil. The latter is defined as $Q \approx \omega_c L/R$, where R is the effective series resistance of the coil. The value of Q for typical coil geometries is typically 50 or higher, so the probe bandwidth is much less than ω_c. The dynamics of such narrow-band probes begins to affect the measurement when ω_c/Q becomes comparable to the NMR signal bandwidth, which is approximately $2\omega_1$ for typical NMR well-logging tools (extended sample in a static field gradient). Here $\omega_1 = \gamma B_1 = \pi/(2T_{90})$ is the nutation frequency, B_1 is the amplitude of the RF magnetic field seen by the spins, and T_{90} is the length of a 90-degree RF pulse. There are two main visible effects of limited probe bandwidth. Firstly, the transmitted pulses cannot be turned on and off abruptly. As a result, their amplitude profiles do not look “rectangular”, but have long rise and fall times. Secondly, NMR signals induced on the coil are band-pass filtered by the probe before they can be amplified, resulting in distorted and time-delayed waveforms at the output of the receiver.

Recently a non-resonant or un-tuned probe circuit has been proposed [1] to eliminate the effects of limited probe bandwidth. In this case a tuning capacitor is not present, and the coil is driven directly by the transmitter. In this report we thoroughly analyze the dynamics of both tuned and un-tuned probe

circuits. We also describe techniques for incorporating such dynamics into the optimization process for phase-modulated RF pulses, which have previously been shown to significantly increase the signal-to-noise ratio (SNR) for a given peak RF power level [2].

Un-tuned probes

An un-tuned NMR probe simply consists of a coil, which can be modeled as an inductor L in series with a resistor R_c. Some parasitic capacitance C_{par} is always present in parallel with the coil, but the resultant self-resonant frequency $\omega_{SRF} = 1/\sqrt{LC_{par}}$ is assumed to be much larger than the Larmor frequency ω_0. In this case the capacitance has negligible effects on the transmitter and receiver dynamics.

Transmitter dynamics

The dynamics of an un-tuned probe during transmission can be studied analytically if we assume a "switched linear" type of model. This modeling approach is common for analyzing power electronics circuits. The circuit is modeled as a collection of N linear networks that can be individually analyzed using standard linear network theory. At certain instants, a controller switches the system between two of these networks. The switching action is assumed to be much faster than the circuit dynamics of interest, i.e., essentially instantaneous. It is also assumed to conserve energy. As a result, switching cannot change the values of any state variables (voltages across capacitors or currents through inductors) in the circuit.

In our case we need only two networks to create a first-order model of the transmitter, as shown in Figure 1 and described below:

1. Transmitter on: The input source is modeled as a sinusoidal voltage source V_{in} in series with a resistor R_s. Note that most low-frequency NMR transmitters actually use a square wave input source. However, only the fundamental component affects the spin dynamics, so it can be replaced by a sinusoidal wave with $4/\pi = 1.27...$ times the amplitude to simplify the analysis. Here the factor of $4/\pi$ comes from a Fourier analysis of the square wave.
2. Transmitter off: The input is modeled as a resistor R_s to ground. The value of R_s can be set to a low value just after an RF pulse to model a "Q-switch". Such circuits consist of switches that quickly dissipate the remaining energy in the coil, thus allowing the receiver to recover faster from saturation.

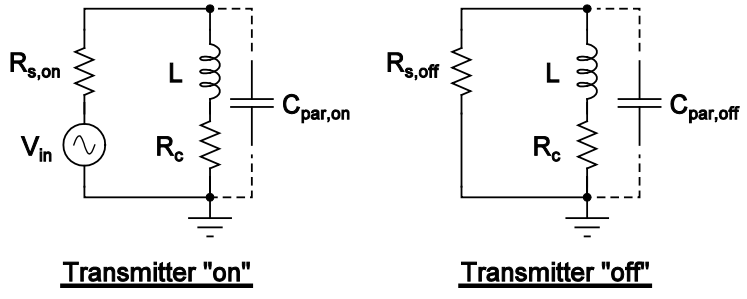

Figure 1: A first-order, two-state model of an un-tuned NMR probe and transmitter.

The relevant circuit equations are identical for both networks if we use the appropriate value of R_s and recognize that $V_{in} = 0$ when the transmitter is off. Using Kirchoff's current law, we have:

$$V_c = L\frac{dI_c}{dt} + R_c I_c$$
$$I_c = \frac{V_{in}(t) - V_c}{R_s}.$$

These equations can be combined into a single first-order differential equation, given by

$$\frac{dI_c}{dt} + \left(\frac{R_s + R_c}{L}\right) I_c = \frac{V_{in}(t)}{L}.$$

In normalized form, this equation becomes

$$\frac{dy}{dt} + \frac{y}{\tau} = f(t).$$

Here $y \equiv I_c$, the time constant $\tau \equiv L/\left(R_c + R_s\right)$, and the input function $f(t) \equiv V_{in}(t)/L$.

Homogeneous solution

We first find a general solution of the associated homogenous equation, obtained by setting $f(t) \to 0$ on the right-hand side. Physically, this corresponds to the natural (not driven) dynamics of the system. The homogeneous equation is given by

$$\frac{dy}{dt} + \frac{y}{\tau} = 0.$$

Its general solution is an exponential decay given by $y_h(t) = y(0)e^{-t/\tau}$. Hence the time constant τ is a measure of how rapidly initial conditions within the coil decay with time.

Particular solution of the driven (inhomogeneous) equation

The second step is to find a particular solution of the inhomogeneous (driven) differential equation. We first only consider one circularly polarized frequency component during RF pulses. It is valid to ignore the other circularly polarized component (which is offset by $\omega + \omega_0 \approx 2\omega_0$ from the Larmor frequency ω_0 and causes the Bloch-Siegert shift) when $\omega_0 \gg \omega_1$. This condition is generally satisfied in our experiments. The input function during RF pulses is then given by

$$f(t) = u(t)e^{i(\omega t + \phi)}.$$

Here ω is the RF frequency, and $u(t)$ is the unit step function. The latter expresses the fact that the input is turned on at t = 0.

We found a particular analytical solution to this problem by using Mathematica's *DSolve* function. The result is

$$\begin{aligned} y_d(t) &= u(t)e^{i\phi}\left(\frac{\tau}{1+i\omega\tau}\right)\left[e^{i\omega t}-e^{-t/\tau}\right] \\ &= u(t)Ae^{j(\phi+\theta)}\left[e^{i\omega t}-e^{-t/\tau}\right]. \end{aligned}$$

Here the sinusoidal steady-state transfer function is defined as $A(\omega)e^{i\theta(\omega)} \equiv \tau/(1+i\omega\tau)$. It has the form of a first-order lowpass filter. It is interesting to note that $\omega\tau = \omega L/(R_c+R_s)$ is the effective quality factor of the un-tuned probe during transmission. This quantity is usually $\gg 1$ at the Larmor frequency, resulting in a steady-state phase-shift $\theta(\omega) \approx -\pi/2$.

General solution

The general solution to the driven differential equation is simply the sum of the homogeneous and particular solutions:

$$\begin{aligned} y(t) &= y_h(t) + y_d(t). \\ &= u(t)Ae^{i(\phi+\theta)}\left[e^{i\omega t}-e^{-t/\tau}\right] + y(0)e^{-t/\tau} \\ &= \underbrace{u(t)Ae^{i(\omega t+\phi+\theta)}}_{\text{Steady state}} + \underbrace{\left(y(0)-u(t)Ae^{i(\phi+\theta)}\right)e^{-t/\tau}}_{\text{Transient}}. \end{aligned}$$

We have decomposed the solution into its asymptotic (steady-state) and transient components.

We are interested in the behavior of this system during a phase-modulated RF pulse. Such broadband pulses, which can be derived using the principles of optimum control theory (OCT), can significantly increase the signal-to-noise ratio (SNR) for a given peak RF power level [2]. We would like to remove the transient components produced by sudden changes in input phase during such phase-modulated pulses. Let's assume that the output has reached its steady-state value before the input phase changes from ϕ to ϕ' at time $t = T$. We can simply change the effective RF phase to $\phi_{eff} = \omega T + \phi$ in order to use the solution we derived earlier (for a step at $t = 0$) in this situation (for a step at $t = T$).

In this case the initial amplitude of the transient component is given by

$$\left(y(T) - Ae^{i(\omega T+\phi'+\theta)}\right) = A\left(e^{i(\omega T+\phi+\theta)} - e^{i(\omega T+\phi'+\theta)}\right) = Ae^{i(\omega T+\theta)}\left(e^{i\phi}-e^{i\phi'}\right).$$

Unfortunately, this quantity is non-zero except for the trivial case of no phase change ($\phi = \phi'$). Therefore the transient component cannot be removed.

However, the situation changes when we have a linearly-polarized input voltage. Such voltage sources are the norm at NMR frequencies up to several hundred MHz. In this case

$$f(t) = u(t)\cos\left(\omega t + \phi\right) = \frac{u(t)}{2}\left[e^{i(\omega t+\phi)} + e^{-i(\omega t+\phi)}\right].$$

The differential equation is linear, so the particular solution in this case can easily be found by superposition. It is given by $\left(y_{d1}(t) + y_{d2}(t)\right)/2$, where $y_{d1}(t)$ is the solution for one circularly polarized component that we found earlier, and $y_{d2}(t)$ is the solution for the other component. The latter can be obtained from the former through the substitutions $\omega \to -\omega$ and $\phi \to -\phi$.

The general solution is now given by

$$\begin{aligned} y(t) &= y_h(t) + \left(y_{d1}(t) + y_{d2}(t)\right)/2. \\ &= y(0)e^{-t/\tau} + u(t)\frac{A}{2}e^{i(\phi+\theta)}\left[e^{i\omega t} - e^{-t/\tau}\right] + u(t)\frac{A}{2}e^{-i(\phi+\theta)}\left[e^{-i\omega t} - e^{-t/\tau}\right] \\ &= \underbrace{u(t)A\cos\left(\omega t + \phi + \theta\right)}_{\text{Steady state}} + \underbrace{\left[y(0) - u(t)A\cos\left(\phi+\theta\right)\right]e^{-t/\tau}}_{\text{Transient}}. \end{aligned}$$

Now the initial amplitude of the transient component for a phase change at time $t = T$ is given by $\left[y(T) - A\cos\left(\omega T + \phi' + \theta\right)\right] = A\left[\cos\left(\omega T + \phi + \theta\right) - \cos\left(\omega T + \phi' + \theta\right)\right]$. The condition for cancelling the transient is then given by

$$\cos\left(\omega T + \phi + \theta\right) = \cos\left(\omega T + \phi' + \theta\right).$$

This equation is satisfied when the steady-state RF waveforms of the previous and current pulse segments cross each other. It has the same trivial solution of no phase change ($\phi = \phi'$) that we found earlier. However, the symmetry of the cosine function about 0 also provides another solution. Since $\cos(x) = \cos(-x)$, the equation is also satisfied if

$$\begin{aligned} &\left(\omega T + \phi + \theta\right) = -\left(\omega T + \phi' + \theta\right) \\ &\Rightarrow \boxed{\omega T = -\frac{\left(\phi + \phi'\right)}{2} - \theta}. \end{aligned}$$

This condition is satisfied twice during each RF cycle. These crossing locations are separated by half a cycle, i.e. by a time ΔT such that $\omega\left(\Delta T\right) = \pm\pi$. In addition, the values of coil current at these crossing points are inverses of each other, because of the fact that $\cos(x \pm \pi) = -\cos(x)$. Thus the transient components can be cancelled by keeping track of the absolute RF phase ωT when the phase is switched, as indicated in Figure 2.

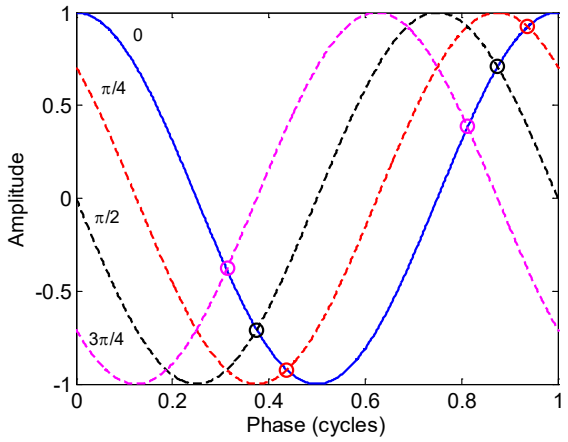

Figure 2: Graphical explanation of the transient elimination principle. The RF waveform corresponding to the initial phase (assumed to be $\phi = 0$) is shown as the solid line, while waveforms corresponding to various phase offsets are shown as dashed lines. It is possible to switch to one of these phases without generating a transient if the switching occurs at the times indicated by circles, i.e., when the initial and final waveforms intersect each other.

The fact that crossing points are separated by half an RF cycle means that the maximum timing adjustment ΔT_{adj} required for phase-switching instants to coincide with crossing points is one quarter of a cycle, i.e., it is sufficient if $\omega\left|\Delta T_{adj}\right| \le \pi/2$. For complex OCT pulses we expect $\omega\left(\Delta T_{adj}\right)$ to be uniformly distributed between $\pm\pi/2$, which results in a standard deviation of $\pi/\left(2\sqrt{3}\right) = 52.0$ degrees.

In broadband pulse design problems it is often convenient to express the crossing condition as

$$\mathrm{mod}\left(\omega T, \pi\right) = \mathrm{mod}\left[-\frac{\left(\phi+\phi'\right)}{2} - \theta, \pi\right] \equiv \alpha.$$

We will write the absolute phase as $\omega T = \pi M + \omega\left(\Delta T_{adj}\right)$, where M is an integer and $\omega\left|\Delta T_{adj}\right| \le \pi/2$. The switching instant for a phase transition can now be adjusted by a small amount ΔT_{adj} to cancel the transient, where

$$\omega\left(\Delta T_{adj}\right) = \begin{cases} \alpha, & \alpha \le \pi/2 \\ -\left(\pi - \alpha\right), & \alpha > \pi/2 \end{cases}.$$

Special conditions are required for the first and last pulse segments, as described below:

1. First segment: In this case the initial condition $y(0) = 0$, so the condition for avoiding a transient is $\cos\left(\omega T + \phi' + \theta\right) = 0$, where ϕ' is the phase of the segment and T is the time at which it begins. This condition may be written as

$$\mathrm{mod}\left(\omega T+\phi'+\theta,\pi\right)=\frac{\pi}{2}\quad\text{or}\quad\mathrm{mod}\left(\omega T+\phi'+\theta,\pi\right)=\frac{3\pi}{2}.$$

In the common case when $\omega T=\pi M$ and $\theta\approx-\pi/2$, these conditions correspond to $\phi'=\{0,\pi\}$. In this case the input voltage reaches its maximum (or minimum) value at $t=T$. The steady-state part of the coil current is in quadrature with this voltage, since $\theta\approx-\pi/2$. It must therefore be zero at $t=T$. In addition, the total coil current must also be zero in order to remain continuous. Hence the transient part of the coil current must also be zero.

2. Last segment: In this case we require the segment to end with zero current in the coil, so that no transient response is excited afterwards. Thus we must have $y(T')=0$, where the time at which the last segment *ends* is denoted by T'. Assuming the current has reached steady state by this point, this condition may be written as $\cos\left(\omega T'+\phi'+\theta\right)=0,$ where ϕ' is the phase of the segment. It may also be expressed as

$$\mathrm{mod}\left(\omega T'+\phi'+\theta,\pi\right)=\frac{\pi}{2}\quad\text{or}\quad\mathrm{mod}\left(\omega T'+\phi'+\theta,\pi\right)=\frac{3\pi}{2}.$$

In practical NMR systems the available phase angles and segment lengths are constrained to vary in discrete steps. The phases are quantized to the set $k\left(2\pi/N_p\right)$, where $0\le k<N_p$ is an integer and N_p is usually a power of two. Pulse segment lengths and delays are similarly quantized to the set $k\left(2\pi/\left(\omega N_t\right)\right)$, resulting in N_t steps per Larmor cycle.

It is easy to see that the quantity $\left(\phi+\phi'\right)/2$ will be quantized to one of $2N_p$ uniformly-spaced values. We assume that the steady-state phase shift θ has also been quantized to this set. Thus the adjustment angle α for transient cancellation will also be quantized to one of $2N_p$ values. As a result we need $2N_p$ time steps per Larmor cycle to cancel the transient, so we must have $N_t=2N_p$. For example, we need 32 steps per cycle to cancel the transients produced by switching between a set of 16 phases.

The transient cancellation condition becomes particularly simple when the phase changes between adjacent pulse segments are constrained to be multiples of π. Examples include RP2 refocusing pulses, other symmetric phase-alternating (SPA) refocusing pulses, and BPP excitation pulses [3]. In this case we have $\phi'=\phi\pm\pi$, so the condition $\cos\left(\omega T+\phi+\theta\right)=\cos\left(\omega T+\phi'+\theta\right)$ can be written as

$$\begin{aligned}&\left(\omega T+\phi+\theta\right)=-\left(\omega T+\phi\pm\pi+\theta\right),\\&\Rightarrow\left(\omega T+\phi+\theta\right)=\pm\frac{\pi}{2}\\&\Rightarrow\cos\left(\omega T+\phi+\theta\right)=0.\end{aligned}$$

Thus, in this case transients are cancelled simply by switching phases when the coil current goes through zero, i.e., at zero-crossings. In addition, it is usually safe to assume that the energy from previous pulses has been completely dissipated before the current pulse begins. Therefore the coil current at the beginning of the pulse must be zero, i.e. the pulse must begin at a zero-crossing. Finally, in order to cancel the transient after the last pulse segment, we require that $\cos\left(\omega T' + \phi' + \theta\right) = 0$. Hence the pulse must also end at a zero-crossing.

We conclude that the beginning, end, and segment transitions of phase-alternating pulses should always occur at zero-crossings. This condition implies that all pulse segment lengths and inter-pulse delays should be integer multiples of half the Larmor period, which considerably simplifies practical implementations of transient cancellation.

The average power dissipated in the coil and transmitter over some duration T is given by

$$\begin{aligned} P_{diss} &= \frac{\left(R_c + R_s\right)}{T}\int_0^T {I_c}^2(t)dt \\ &= \frac{\left(R_c + R_s\right)}{T}\int_0^T \left[I_{ss}\cos\left(\omega t + \theta + \phi'\right) + I_{tran}e^{-t/\tau} \right]^2 dt. \end{aligned}$$

Here $I_{ss} = A\left(V_{in}/L\right) = V_{in}/\left(R\sqrt{\omega^2\tau^2+1}\right)$ is the steady-state current amplitude in the coil, while $I_{tran} = I_c(0) - I_{ss}\cos(\theta+\phi')$ is the initial amplitude of the transient component. We assume that the integration is performed over many RF cycles, such that $\omega T \gg 1$. The average power dissipation is then given by

$$P_{diss} \approx \left(R_c + R_s\right)\left[\frac{I_{ss}^2}{2} + {I_{tran}}^2\left(\frac{1-e^{-2T/\tau}}{2T/\tau}\right)\right].$$

We assume that the previous pulse segment has reached steady state. In this case the initial amplitude of the transient component can be written as $I_{tran} \approx I_{ss}\left[\cos(\theta+\phi) - \cos(\theta+\phi')\right]$. We also assume that the initial and final phases (ϕ and ϕ', respectively) are uniformly distributed and uncorrelated random variables. In that case the variance of I_{tran} can be written as

$$\overline{I_{tran}^2} = {I_{ss}}^2\left[\overline{\cos\left(\theta+\phi\right)^2} + \overline{\cos\left(\theta+\phi'\right)^2}\right] = I_{ss}^2\left[\frac{1}{2}+\frac{1}{2}\right] = I_{ss}^2.$$

The expected value of the average power dissipation is then given by

$$\overline{P_{diss}} \approx \left(R_c + R_s\right)\frac{I_{ss}^2}{2}\left[1 + 2\left(\frac{1-e^{-2T/\tau}}{2T/\tau}\right)\right].$$

The fractional increase in power dissipation due to the modulation is simply given by the function $1+2\left(1-e^{-x}\right)/x$, where $x \equiv 2T/\tau$. For example, if $T \approx \tau$ we have $x = 2$, so the expected fractional increase in power dissipation is 86.5%.

NMR spin dynamics are usually calculated in a frame that rotates about the static field (*z*-axis) at the Larmor frequency ω_0. The coil current in this frame can be calculated by "demodulating" the RF coil current, as follows:

$$I_{cr}(t) = I_c(t)e^{-i\omega_0 t}.$$

In most cases the input frequency $\omega \approx \omega_0$, resulting in a rotating-frame coil current with three main components:

1. Centered on DC: This component has an amplitude of $I_{ss}/2$, and is responsible for most of the interesting spin dynamics.
2. Centered on $2\omega_0$: This component has an amplitude of $I_{ss}/2$, and is responsible for the Bloch-Siegert shift. This effect is negligible when $\omega_1 \ll \omega_0$, as is usually the case. We can eliminate it from spin dynamics simulations by averaging $I_{cr}(t)$ over segments of length $1/(2\omega_0)$ before feeding it into the simulator.
3. Centered on ω_0: This component is produced by the probe transients. It has an amplitude of $I_{tran}/2$, and its effects on the spin dynamics are usually negligible when $\omega_1 \ll \omega_0$.

The time-varying magnetic field acting on the spins in the rotating frame can now be found by scaling I_{cr} by the coil sensitivity, i.e., we can write $B_{1r}(t) = (B_1/I_1)I_{cr}(t)$. This field can be directly fed into spin dynamics simulators.

The effectiveness of the transient elimination method is shown by the following example. We assume an un-tuned probe with $L = 15\ \mu\text{H}$, $R_c = 0.4\ \Omega$, and a source resistance of $R_s = 1.5\ \Omega$ in both states (transmitter "on" or "off"). Thus the transmitter time constant is equal to $\tau = 15/(0.4+1.5) = 7.9\ \mu\text{s}$. The Larmor frequency is assumed to be 500 kHz, corresponding to a coil quality factor of $Q = (\omega_0 L)/R_c = 117.8$. We want to feed a phase-modulated, constant-amplitude OCT excitation pulse into the probe. The pulse has 180 segments, each of length $T = 8\ \mu\text{s}$. We therefore expect the transmitter power dissipation to increase by a factor of about $1+2\left(1-e^{-x}\right)/x = 1.857$ (where $x \equiv 2T/\tau = 2.027$) if the transients are not eliminated.

We assume that the pulse phases have been quantized to one of $N_p = 16$ uniformly-spaced values. In order to cancel transients we therefore need a timing precision of $2N_p = 32$ points per Larmor cycle, which corresponds to a clock frequency of 0.5 x 32 = 16 MHz. Figure 3 shows the normalized segment

lengths required to eliminate the probe transients in this case. The adjusted length of a given segment is no longer constant, but varies slightly depending on its own phase, the phase of all previous segments, and the phase of the next segment. The resultant standard deviation in segment lengths is found to be only 0.29 μs, which is 3.7% of its nominal value. This value is in excellent agreement with the theoretical result, which is $\pi / \left(2\sqrt{3}\omega_0\right) = 0.29\,\mu\text{s}$.

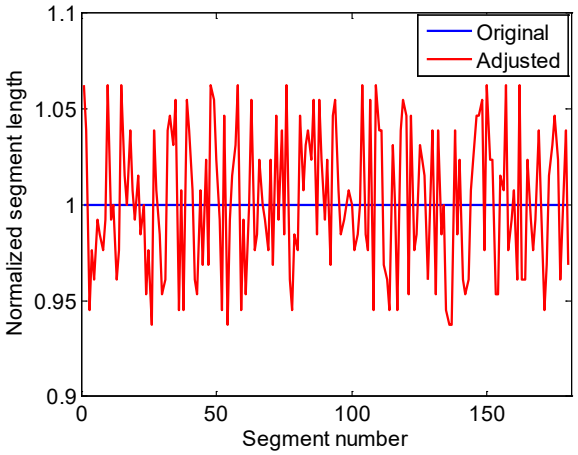

Figure 3: Normalized segment lengths of the OCT pulse described in the text after adjustment to eliminate probe settling transients.

Figure 4 shows the simulated coil current with and without transient cancellation. The power dissipated in the coil is 65.4% higher in the latter case. This number is in good agreement with the expected value of 85.7%. In addition, without transient cancellation the peak current in the coil is almost 2.5 times larger than its average value. Such large currents are undesirable – they can blow fuses or damage the transmitter electronics.

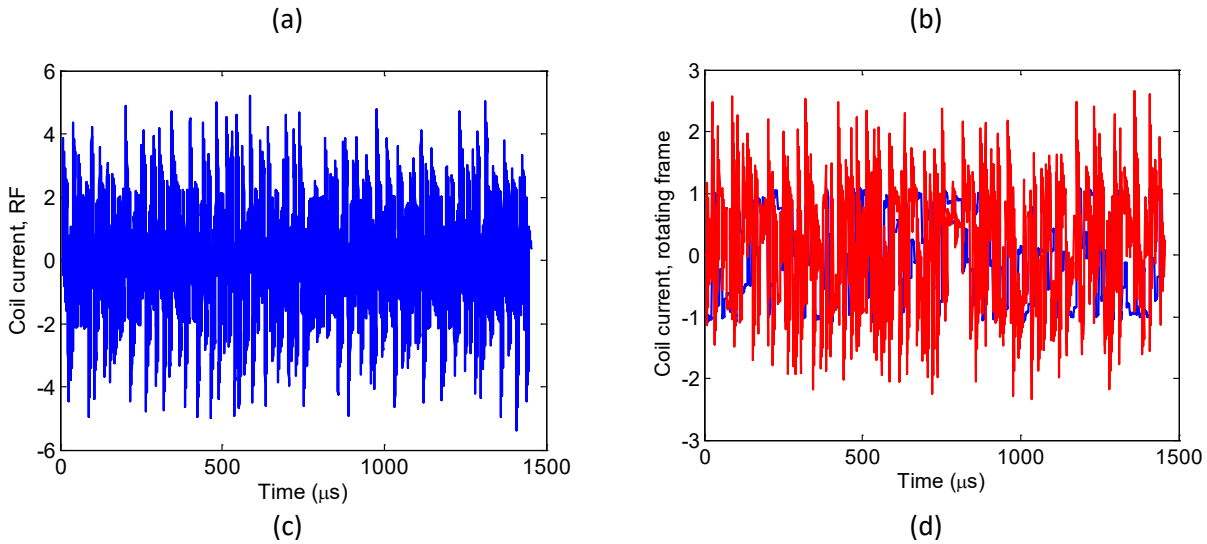

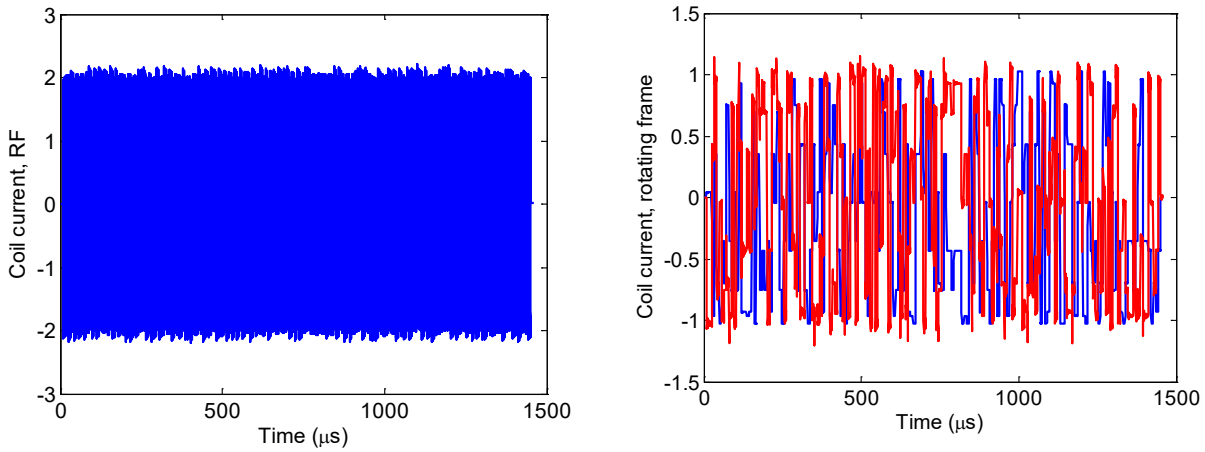

Figure 4: Simulated coil current during the OCT pulse described in the text without transient cancellation (shown in (a) and (b)), and with transient cancellation (shown in (c) and (d)). In either case the plot on the left shows the RF coil current, while the plot on the right shows the real and imaginary components of the coil current in the rotating frame, i.e., after demodulation with the Larmor frequency. All results have been normalized to a steady-state current magnitude of unity in the rotating-frame. This allows the latter to be directly fed into a spin dynamics simulator to calculate the NMR response.

Non-sinusoidal coil currents

Many low-frequency NMR transmitters are switch-based and produce substantial amounts of harmonic distortion, so the fundamental-only analysis presented so far is not strictly applicable to them. In this case the driving function should be expressed as a Fourier series:

$$f(t) = u(t)\sum_{n=1}^{\infty} a_n e^{in(\omega t+\phi)}.$$

Here the coefficients a_n depend on the shape of the transmitter voltage waveform. Note that we have implicitly assumed that the average (DC) term is zero by starting the series from $n=1$. Using superposition, the general solution for coil current is now given by

$$\begin{aligned} y(t) &= y_h(t) + \left(y_{d1}(t) + y_{d2}(t)\right)/2. \\ &= y(0)e^{-t/\tau} + u(t)\sum_{n=1}^{\infty}\frac{A_n a_n}{2}e^{i(n\phi+\theta_n)}\left[e^{in\omega t} - e^{-t/\tau}\right] + u(t)\sum_{n=1}^{\infty}\frac{A_n a_n}{2}e^{-i(n\phi+\theta_n)}\left[e^{-in\omega t} - e^{-t/\tau}\right] \\ &= \underbrace{u(t)\sum_{n=1}^{\infty}A_n a_n\cos\left(n\left(\omega t+\phi\right)+\theta_n\right)}_{\text{Steady state}} + \underbrace{\left[y(0) - u(t)\sum_{n=1}^{\infty}A_n a_n\cos\left(n\phi+\theta_n\right)\right]e^{-t/\tau}}_{\text{Transient}}. \end{aligned}$$

Here $A_n e^{i\theta_n} \equiv \tau/\left(1+in\omega\tau\right)$ is the transfer function between transmitter voltage and coil current for the *n*-th harmonic of the fundamental frequency. Assuming that the previous pulse segment has reached steady-state, the condition for transient cancellation at $t=T$ is given by

$$\sum_{n=1}^{\infty}A_n a_n\cos\left(n\left(\omega T+\phi\right)+\theta_n\right) = \sum_{n=1}^{\infty}A_n a_n\cos\left(n\left(\omega T+\phi'\right)+\theta_n\right).$$

This equation requires the two steady-state waveforms to cross each other at the switching instant $t = T$. In general it must be solved numerically. However, the situation is considerably simplified if $\theta_n \approx -(\pi/2)\ \forall n$ and the coil current contains only odd harmonics. Both requirements are usually satisfied in practice. The first only requires that $\omega\tau \gg 1$, while the second requires the coil current to have *half-wave symmetry.* In this case the waveform is anti-symmetric about zero within every cycle, i.e., it has positive and negative half-cycles that are equal in amplitude and opposite in sign. More precisely, it satisfies the condition $y(t \pm T/2) = -y(t)$ where $T = 2\pi/\omega$ is the period of the fundamental component. For two-phase switching transmitters such as H-bridges and half-bridges, the half-wave symmetry condition is satisfied if identical switching waveforms are used for both phases within a single RF cycle. In such cases a symmetric square wave voltage waveform is applied across the coil, so the coil current becomes a triangle wave.

If both of these requirements are satisfied, the condition for eliminating transients at $t = T$ can be written as

$$\sum_{n=1}^{\infty} \frac{a_n}{n\omega} \cos\left(n(\omega T + \phi) - \frac{\pi}{2} \right) = \sum_{n=1}^{\infty} \frac{a_n}{n\omega} \cos\left(n(\omega T + \phi') - \frac{\pi}{2} \right).$$

Here we have used the fact that $A_n \approx 1/(n\omega)\ \forall n$ if $\omega\tau \gg 1$. We also note that $\cos\left(n(\omega T \pm \pi + \phi) - \pi/2\right) = -\cos\left(n(\omega T + \phi) - \pi/2\right)$ for any odd value of *n*, so there are still two solutions within each RF cycle that are separated by $\omega T = \pi$ (although there may be more). In addition, we see that

$$\cos\left(n(\omega T + \phi) - \frac{\pi}{2} \right) = \begin{cases} \cos\left(n\left(\omega T + \phi - \frac{\pi}{2} \right) \right), n = 1,5,9... \\ -\cos\left(n\left(\omega T + \phi - \frac{\pi}{2} \right) \right), n = 3,7,11... \end{cases}$$

We can therefore write the condition for transient cancellation as

$$\sum_{n=1}^{\infty} \frac{a_n (-1)^{(n-1)/2}}{n\omega} \cos\left(n\left(\omega T + \phi - \frac{\pi}{2} \right) \right) = \sum_{n=1}^{\infty} \frac{a_n (-1)^{(n-1)/2}}{n\omega} \cos\left(n\left(\omega T + \phi' - \frac{\pi}{2} \right) \right).$$

Since $\cos(x) = \cos(-x)$ for any value of *x*, this equation will be satisfied for the *n*-th harmonic if the corresponding phases on both sides are inverses of each other, i.e., if

$$\begin{aligned} & n(\omega T + \phi - \pi/2) = -n(\omega T + \phi' - \pi/2) \\ \Rightarrow\ & (\omega T + \phi - \pi/2) = -(\omega T + \phi' - \pi/2). \end{aligned}$$

The latter condition is independent of the value of *n*. Moreover, it is identical to the condition we derived earlier for the sinusoidal case (after substituting $\theta = -\pi / 2$). As a result, waveform crossing locations are unaffected by the presence of harmonics, and we can cancel coil current transients by applying exactly the same timing corrections that were earlier derived for the fundamental component. However, the amount of transmitter power saved by this procedure will depend on the shape of the transmitter waveform.

Speeding up the transient response

It may not always be possible to eliminate coil current transients. For example, there may be insufficient timing precision available. In this case other techniques can be used to reduce the settling time following a phase transition. Settling dynamics can be studied by modeling the un-tuned probe as a series L-R circuit driven by a voltage source, as shown on the left-hand side of Figure 5. The transfer function between this input voltage source and the coil current is simply that of a first-order low-pass filter, as described earlier.

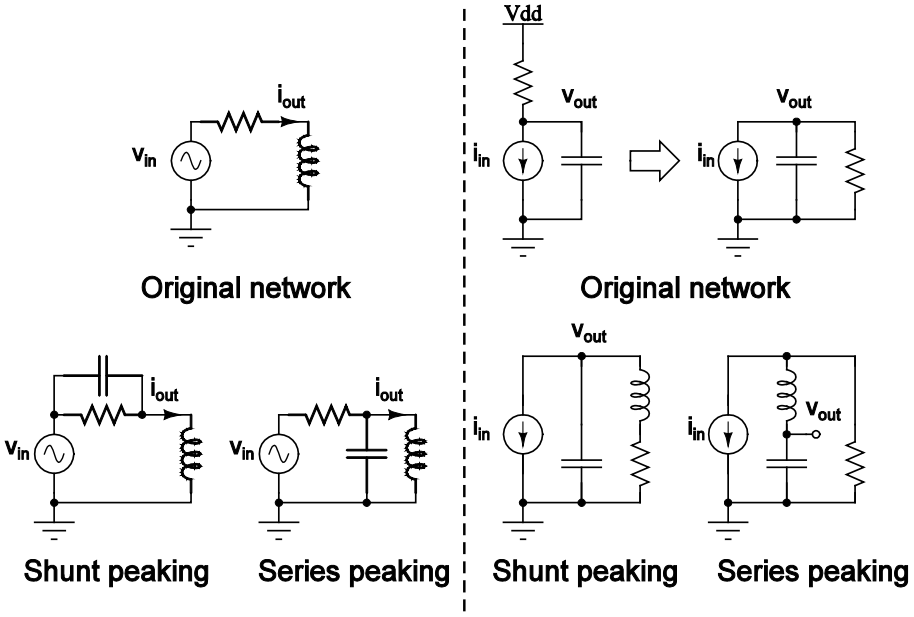

Figure 5: Some common "peaking" networks. Typical networks used in transistor amplifiers are shown on the right, while their duals are shown on the left. The latter can be used for speeding up the transient response of un-tuned NMR probes.

The simplest method of reducing the settling time of this circuit is to increase the value of the series resistor. This causes the time constant $\tau = L / R$ to decrease at the cost of increased power consumption. Such increases are undesirable, so we consider alternative approaches.

Any linear electrical network can be converted into a "dual network" through a series of well-defined transformations. In particular, these transformations involve the interchange of current and voltage sources, inductors and capacitors, and series and parallel connections. The dynamics of the resultant dual network are identical to the original network, but with currents replaced by voltages and vice versa. The dual of our un-tuned probe model is a current source driving a parallel R-C network, as shown on the right-hand side of Figure 5. Interestingly, this circuit is identical to that used to model broadband

transistor-based amplifiers. The input current source in this circuit represents the small-signal trans-conductance of the transistor, the resistor sets the voltage gain, and the capacitor represents the output load.

The theory of such broadband amplifiers is well-understood. For example, it is known that adding passive components (typically inductors) to the circuit can increase its bandwidth, or equivalently reduce its settling time, without increasing DC power consumption. Such bandwidth-extension techniques are often known as "peaking". The general idea is to use the added inductor(s) to delay the charging of the output capacitor, thus trading off propagation delay versus rise time and small-signal bandwidth. The logical culmination of this process involves dividing the load capacitor into many small parts (in parallel) and inserting inductors between them (in series) – thus forming a transmission line with ideally infinite bandwidth.

The two most common methods of using a single inductor for peaking are shown on the right-hand side of Figure 5. These methods are known as series and shunt peaking, respectively. The corresponding dual networks, which are applicable to un-tuned NMR probes, are shown on the left-hand side of Figure 5. However, in the case of an NMR probe the input (RF) frequency is usually much larger than the bandwidth of the L-R low-pass filter. We would like to keep the RF response unchanged, so our peaking network should not modify the high-frequency transfer function of the circuit. Only the shunt peaking circuit satisfies this requirement, so we will now focus on it. It should be noted that this requirement is not relevant for a transistor amplifier, because it is only meant to amplify input frequencies that are smaller than its bandwidth. Hence its high-frequency transfer function is of little interest, and can be modified by the peaking network.

Figure 5 predicts that a shunt-peaked, un-tuned NMR probe can be constructed by simply adding a capacitor across the resistance in series with the input voltage source. A more realistic model of such a probe is shown in Figure 6. The series resistor has been divided into two components: R_c, which represents losses in the coil, and R_1, which represents the equivalent resistance of the voltage source. A resistor R_2 has also been added in series with the shunt-peaking capacitor C to model losses within this branch of the circuit.

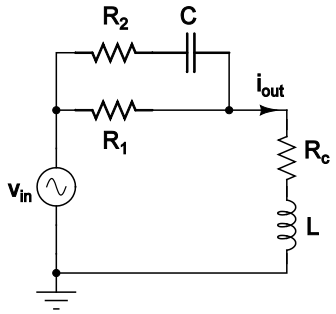

Figure 6: A more realistic shunt-peaking network for an un-tuned NMR probe.

The shunt-peaked circuit shown in Figure 6 satisfies the following equations, which can be derived using Kirchoff's current laws (KCL):

$$i_{out} = \frac{v_{out}}{sL + R_c},$$

$$i_{out} = \left(v_{in} - v_{out}\right)\left(\frac{sC}{sCR_2 + 1} + \frac{1}{R_1}\right).$$

We can solve these equations to calculate the transfer function i_{out} / v_{in}:

$$\frac{i_{out}}{v_{in}} = \frac{1}{R_{dc}}\left(\frac{s\tau_z + 1}{s^2\tau^2 + s\tau / Q + 1}\right).$$

Here we have used the following definitions:

$$R_{dc} = \left(R_c + R_1\right),\ \tau = \sqrt{LC\left(\frac{R_1 + R_2}{R_{dc}}\right)},\ \tau_z = C\left(R_1 + R_2\right),$$

$$Z_0 = \sqrt{L / C},\ Q = \sqrt{\frac{R_{dc}}{\left(R_1 + R_2\right)}}\left[\frac{Z_0}{\left(R_1 + R_2\right)} + \frac{\left(R_c + R_1 \,||\, R_2\right)}{Z_0}\right]^{-1}.$$

The original transfer function was a first-order low-pass filter with time constant $\tau_0 = L / R_{dc}$. Shunt-peaking adds a zero and a pole to this response. It now has two poles, described by time constant τ and quality factor Q, and a single zero with time constant τ_z. It is easy to verify that these changes do not affect the high-frequency behavior ($s \to \infty$) of the transfer function, as expected. However, they can be used to increase the low-frequency bandwidth of the circuit and reduce its settling time.

If $R_2 = 0$ these expressions can be simplified to

$$\tau_z = CR_1,\quad \tau^2 = LC\left(\frac{R_1}{R_{dc}}\right),\quad Q = \sqrt{\frac{R_{dc}}{R_1}}\left[\frac{Z_0}{R_1} + \frac{R_c}{Z_0}\right]^{-1},\quad \frac{\tau}{Q} = \left(\frac{R_1}{R_{dc}}\right)\left[\frac{L}{R_1} + CR_c\right].$$

The corresponding differential equation is given by

$$\tau^2\frac{di_{out}{}^2}{dt^2} + \left(\frac{\tau}{Q}\right)\frac{di_{out}}{dt} + 1 = \frac{1}{R_{dc}}\left(v_{in} + \tau_z\frac{dv_{in}}{dt}\right).$$

This second-order differential equation is that of a damped harmonic oscillator. The main effect of the peaking capacitor is to add the second driving term on the right-hand side. This term is proportional to the derivative of the input voltage, and is responsible for the zero in the transfer function. It becomes large when the input changes rapidly, thus speeding up the recovery of the system to sudden perturbations. The step response of the system shows evidence of this speedup mechanism.

It is convenient in both series- and shunt-peaking networks to define the dimensionless parameter

$$m = \frac{C\left(R_1 + R_2\right)}{\left(L / R_1\right)}.$$

This parameter is the ratio of the two time constants of interest in the circuit. In the limit $m \to 0$ the circuit reduces to the original (non-peaked) form, while as m gets large the response becomes more and more under-damped (oscillatory). If we ignore R_c and perform some algebra, we find that

$$Q = \left[\frac{1}{\sqrt{m}} + \frac{\sqrt{m}}{1 + R_1 / R_2}\right]^{-1}.$$

In the classical shunt peaking circuit $R_2 = 0$, so the expression above reduces to $Q = \sqrt{m}$. Further analysis of this ideal case shows that a maximally flat amplitude response is obtained in the pass-band when $m = \sqrt{2} - 1 \approx 0.414$, which results in $Q = \sqrt{\sqrt{2} - 1} \approx 0.644$. The resultant circuit has 72% more 3 dB bandwidth than the original (non-peaked) circuit, and almost half the rise time during a step response. Smaller values of m produce smaller increases in bandwidth, but the resulting time-domain responses have less envelope distortion and group delay.

In our case we will probably have $R_2 \neq 0$, since the voltage at the source end of the capacitor must be generated using the same mechanism used to generate v_{in}. The latter is often created by periodically inverting the polarity of a DC voltage source using MOSFET switches that are connected in a full- or half-bridge configuration. In this case R_1 and R_2 represent the on-state resistance of the switches. The relevant expression for Q shows that the main effect of non-zero R_2 is to increase the value of m (and hence the size of the peaking capacitor) required to obtain a given value of Q. In addition, Q is limited to a maximum value of

$$Q_{max} = \frac{\sqrt{1 + R_1 / R_2}}{2},$$

which occurs at $m_{max} = \left(1 + R_1 / R_2\right)$. Let us make the reasonable assumption that similar switches will be used for both input paths, so that $R_1 = R_2$. The maximum possible value of Q in this case is $1/\sqrt{2}$, which occurs when $m = 2$. In addition, since $Q = \left(1/\sqrt{m} + \sqrt{m}/2\right)^{-1}$, the previously-discussed value of $Q \approx 0.644$ is now obtained when $m \approx 0.83$. However, this value of Q no longer corresponds to a maximally-flat amplitude response, since the value of τ_z also depends on R_2.

The simulated bandwidth and settling time of the shunt-peaked network are shown as a function of m in Figure 7. Bandwidth is defined as the frequency at which the magnitude of the transfer function reaches -3dB. Settling time is defined as the time after which the system output stays within a specified percentage (in this case, 5%) of its final value. We see that the increase of bandwidth relative to the

non-peaked case $(m = 0)$ decreases as R_2 increases. A similar, but less prominent trend is seen in the settling times. In addition, the values of m required to obtain the best possible performance (maximum bandwidth or minimum settling time) also increase with R_2. Hence we need more shunt capacitance than in the ideal case ($R_2 = 0$) in order to maximize performance.

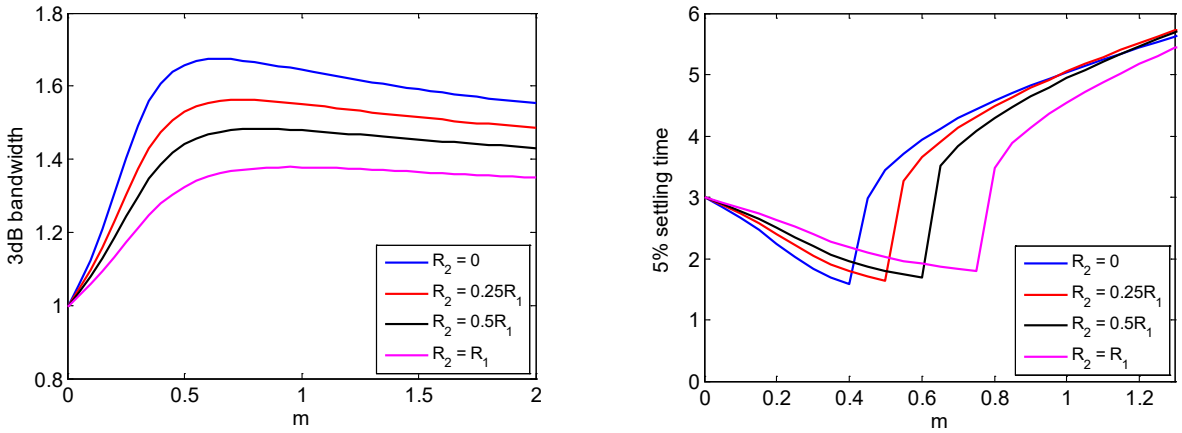

Figure 7: Simulated bandwidth (left) and settling time (right) of the shunt-peaking network for various values of R_2/R_1. The following parameter values were assumed: L = 1, R_1 = 0.75, and R_c = 0.25.

In the practical case when $R_1 = R_2$ the maximum bandwidth of 1.38 occurs when $m \approx 1$, while the minimum settling time of 1.81 occurs when $m \approx 0.8$. These values are 38% higher and 40% lower than in the non-peaked case, respectively.

A possible transistor-level circuit implementation of the shunt-peaked probe and transmitter is shown in Figure 8. The original transmitter consists of four MOSFETs connected as an H-bridge. Shunt-peaking is implemented by adding a capacitor and MOSFET in parallel with each of the four FETs in the bridge. It should be noted that the peaking capacitor *C* must hold a lot of charge. Hence it must have both a large capacitance and a high voltage rating, making it challenging to implement.

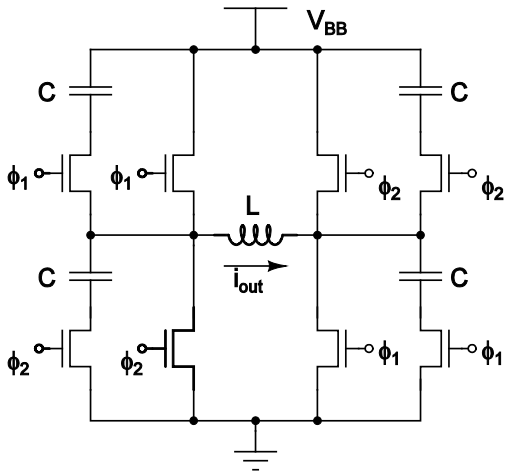

Figure 8: Simplified schematic of a shunt-peaked un-tuned NMR probe and transmitter circuit.

We carried out SPICE simulations of an un-tuned coil and transmitter to verify our theoretical predictions. We used the H-bridge topology shown in Figure 8 with and without the shunt-peaking capacitor *C*. A resistor-capacitor-diode (RCD) snubber circuit was connected in parallel with the H-bridge for over-voltage protection. Other circuit parameters are listed in the table below:

Component	Role	Details
FDC2612 (Fairchild)	H-bridge MOSFET	200 V, R_{on} = 1.1 Ω at 4 A
RCD snubber	Protection	100 Ω || BAS321 diode, in series with 100 pF
IR2011 (International Rectifier)	Half-bridge driver	
BAS321 (NXP)	Cross-coupled diode pairs (x 2)	Isolate transmitter from receiver after turn-off (extender)

The results of our simulations are shown in Figure 9 for a transmitter voltage of 200 V and a coil inductance of 15 µH. The input voltage consisted of two pulse segments, each of length 20 µs, with phases equal to $\pi/2$ and $-\pi/2$, respectively. These phases were selected in order to maximize the amplitudes of the resulting coil current transients.

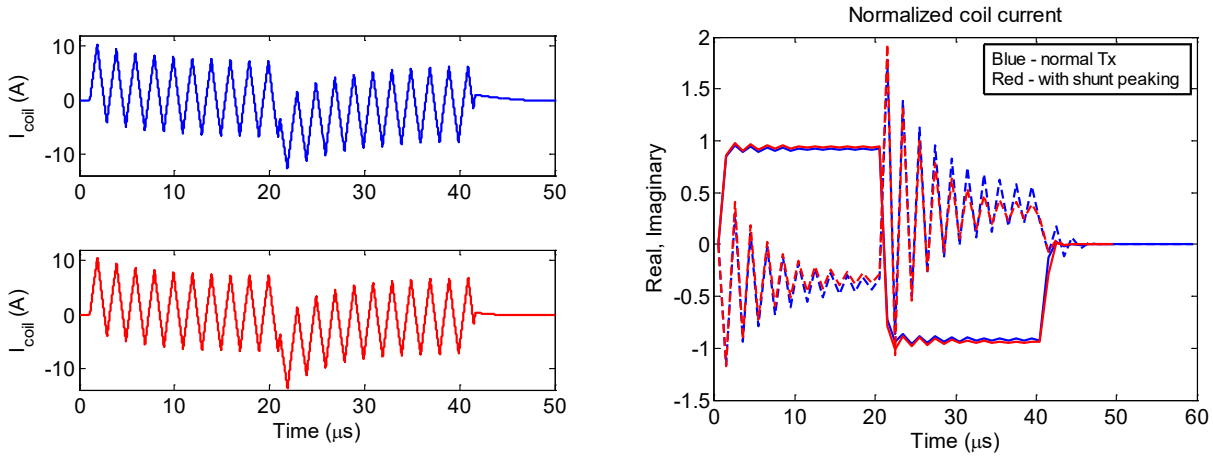

Figure 9: SPICE simulation results of an un-tuned NMR probe with and without shunt-peaking (shown in red and blue, respectively). The RF current in the coil is shown on the left, and the demodulated current in the rotating frame is shown on the right. The input voltage consisted of two pulse segments, each of length 20 µs, with phases = $\pi/2$ and $-\pi/2$, respectively. Simulation parameters: L = 15 µH, $R_c \approx 0.2\ \Omega$, V_{BB} = 200 V, and $\omega_0 = 2\pi$ x 500 kHz. The shunt-peaking capacitor was C = 1 µF, which corresponds to $m \approx 1$.

Figure 9 shows that the shunt-peaked transmitter has substantially faster settling time, as expected. This improvement is particularly noticeable in the rotating frame, where the coil transients appear as rapidly-oscillating sinusoids (centered on ω_0). These signals decay significantly faster when shunt-peaking is present.

Receiver dynamics

We consider the situation after the probe and receiver have recovered from the effects of an RF pulse. The effects of any probe on the NMR signal can then be expressed as a linear time-invariant (LTI) filter $G_R(\omega) \equiv S(\omega) / S_c(\omega)$. Here $S(\omega)$ and $S_c(\omega)$ are the signal spectra induced on the coil and across

the receiver input terminals, respectively. In the case of an unturned probe $G_R(\omega)$ can be assumed to be constant over the bandwidth of interest. For a more detailed analysis, please see [1].

Tuned probes

A tuned NMR probe adds a tuning capacitor *C* in parallel with the coil to form a LC "tank" circuit. The tank circuit acts a narrowband impedance transformer. It provides voltage gain to the induced NMR signal near its resonant frequency, which lowers the noise figure (NF) of the receiver.

Transmitter dynamics

The dynamics of a tuned probe during transmission can be studied analytically by assuming the same two-state "switched linear" model that we used for the un-tuned probe. The model is shown in Figure 10. The relevant circuit equations (using Kirchoff's current law) are

$$V_c = L\frac{dI_c}{dt} + R_c I_c$$
$$C\frac{dV_c}{dt} + I_c = \frac{V_{in}(t) - V_c}{R_s}.$$

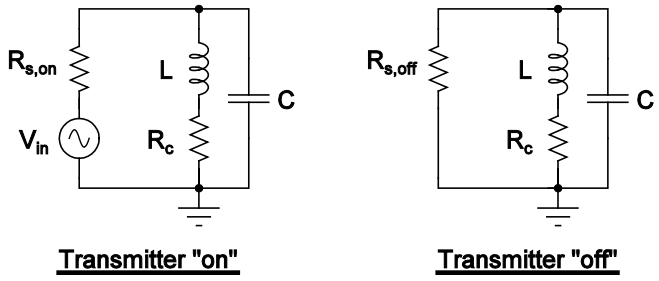

Figure 10: A first-order, two-state model of a tuned NMR probe and transmitter.

These first-order differential equations can be combined into a single second-order differential equation, given by

$$LC\frac{d^2 I_c}{dt^2} + \left(R_c C + \frac{L}{R_s}\right)\frac{dI_c}{dt} + \left(1 + \frac{R_c}{R_s}\right) I_c = \frac{V_{in}(t)}{R_s}.$$

It is convenient to define a dimensionless time variable $\tau \equiv \omega_p t = t/\sqrt{LC}$, and the characteristic impedance of the tuned circuit $Z_0 \equiv \sqrt{L/C}$. In terms of these variables the equation is written as

$$\frac{d^2 I_c}{d\tau^2} + \left(\frac{R_c}{Z_0} + \frac{Z_0}{R_s}\right)\frac{dI_c}{d\tau} + \left(1 + \frac{R_c}{R_s}\right) I_c = \frac{V_{in}(t)}{R_s}.$$

It is now evident that the equation is mathematically identical to that of a driven, damped harmonic oscillator, which is given by

$$\frac{d^2y}{dt^2} + 2\gamma\frac{dy}{dt} + \omega_n^2 y = f(t).$$

Here we have written τ as t for convenience, and also made the following identifications: $y \equiv I_c$, $\omega_n \equiv \sqrt{1+\frac{R_c}{R_s}}$, $\gamma \equiv \frac{1}{2}\left(\frac{R_c}{Z_0}+\frac{Z_0}{R_s}\right)$, and $f(t) \equiv \frac{V_{in}(t)}{R_s}$. Physically, ω_n is the natural oscillation frequency of the circuit, γ is the damping coefficient, and $f(t)$ is the input (driving function). We see that the damping coefficient γ increases as R_s decreases. Many low-frequency NMR transmitters are based on MOSFETs operated as switches. The equivalent source resistance R_s of such a transmitter is approximately equal to the on-resistance of its switches. This is usually a very low value (less than a few Ohms), resulting in a large value of γ. In this case the probe is "over-coupled" to the source, which suppresses its internal dynamics. The result is rapid pulse rise and fall times at the expense of lower steady-state current.

Over-coupling occurs if R_s is smaller than the effective parallel resistance of the LC circuit at resonance (i.e., $\omega = \omega_p$). The latter is given by $R_c Q^2 = Z_0^2 / R_c$ where Q is the quality factor of the coil. The borderline "critically-coupled" case corresponds to $R_s = Z_0^2 / R_c$, which results in a critical damping coefficient of $\gamma_c = R_c / Z_0$.

The general solution of the differential equation can be found in two steps, as described next.

Homogeneous solution

We first find a general solution of the associated homogenous equation, obtained by setting $f(t) \to 0$ on the right-hand side. Physically, this corresponds to the natural (not driven) dynamics of the system. The homogeneous equation is given by

$$\frac{d^2y}{dt^2} + 2\gamma\frac{dy}{dt} + \omega_n^2 y = 0.$$

Its general solution is the sum of two exponential functions, where the coefficients c_1 and c_2 depend on the initial conditions:

$$y_h(t) = c_1 e^{\lambda_1 t} + c_2 e^{\lambda_2 t}$$
$$\dot{y}_h(t) = c_1\lambda_1 e^{\lambda_1 t} + c_2\lambda_2 e^{\lambda_2 t}.$$

By substituting the solution in the differential equation, we find that the exponential rates λ_1 and λ_2 must satisfy the following quadratic equation:

$$\lambda^2 + (2\gamma)\lambda + \omega_n^2 = 0.$$

This equation has the following solutions:

$$\lambda_{1,2} = -\gamma \pm \sqrt{\gamma^2 - \omega_n^2} \equiv -\gamma \pm \alpha.$$

In order to complete the solution we must find the coefficients c_1 and c_2 based on specified initial conditions (values of y and dy/dt at t = 0). They can be found by solving the following set of linear equations:

$$\begin{bmatrix} y_h(0) \\ \dot{y}_h(0) \end{bmatrix} = \begin{bmatrix} 1 & 1 \\ \lambda_1 & \lambda_2 \end{bmatrix} \begin{bmatrix} c_1 \\ c_2 \end{bmatrix}$$

$$\Rightarrow \begin{bmatrix} c_1 \\ c_2 \end{bmatrix} = \begin{bmatrix} 1 & 1 \\ \lambda_1 & \lambda_2 \end{bmatrix}^{-1} \begin{bmatrix} y_h(0) \\ \dot{y}_h(0) \end{bmatrix} = \frac{1}{(\lambda_2 - \lambda_1)} \begin{bmatrix} \lambda_2 & -1 \\ -\lambda_1 & 1 \end{bmatrix} \begin{bmatrix} y_h(0) \\ \dot{y}_h(0) \end{bmatrix} = \frac{1}{2\alpha} \begin{bmatrix} -\lambda_2 y_h(0) + \dot{y}_h(0) \\ \lambda_1 y_h(0) - \dot{y}_h(0) \end{bmatrix}.$$

Particular solution of the driven (inhomogeneous) equation

The second step is to find a particular solution of the inhomogeneous (driven) differential equation. We only consider only one circularly polarized frequency component during RF pulses. It is valid to ignore the other circularly polarized component (which is offset by $\omega + \omega_0 \approx 2\omega_0$ from the Larmor frequency ω_0 and causes the Bloch-Siegert shift) when $\omega_0 \gg \omega_1$. This condition is generally satisfied in our experiments. The input function during RF pulses is then given by

$$f(t) = u(t) e^{i(\omega t + \phi)}.$$

Here ω is the RF frequency, and $u(t)$ is the unit step function. The latter expresses the fact that the input is turned on at t = 0.

We found a particular analytical solution to this problem by using Mathematica's *DSolve* function. The result is given below. The parameter $\alpha \equiv \sqrt{\gamma^2 - \omega_n^2}$, as defined earlier.

$$y_d(t) = u(t) \frac{e^{i\phi - (\gamma+\alpha)t} \left[(i\omega + \gamma)\left(1 - e^{2\alpha t}\right) + \alpha\left(-1 - e^{2\alpha t} + 2e^{(i\omega+\gamma+\alpha)t}\right) \right]}{2\alpha \left[\left(\omega_n{}^2 - \omega^2\right) + 2i\gamma\omega \right]}$$

$$\dot{y}_d(t) = \frac{i e^{i\phi - (\gamma+\alpha)t} \left[\left(i\omega_n^2 - \gamma\omega\right)\left(1 - e^{2\alpha t}\right) + \alpha\omega\left(-1 - e^{2\alpha t} + 2e^{(i\omega+\gamma+\alpha)t}\right) \right]}{2\alpha \left[\left(\omega_n{}^2 - \omega^2\right) + 2i\gamma\omega \right]}, \quad t \geq 0.$$

As an example, the real and imaginary parts of y and dy/dt corresponding to these expressions are shown in Figure 11 for the following set of parameters: $\phi = 0$, $\omega_n = 1$, $\omega = 1.1$, and $\gamma = \{0.1, 0.2, \ldots 0.9\}$. Each solution starts from zero and then builds up to a steady-state over a few cycles. This build-up (or

settling) period is of great interest for NMR applications, since it determines the maximum rate at which the RF pulse can be amplitude or phase modulated.

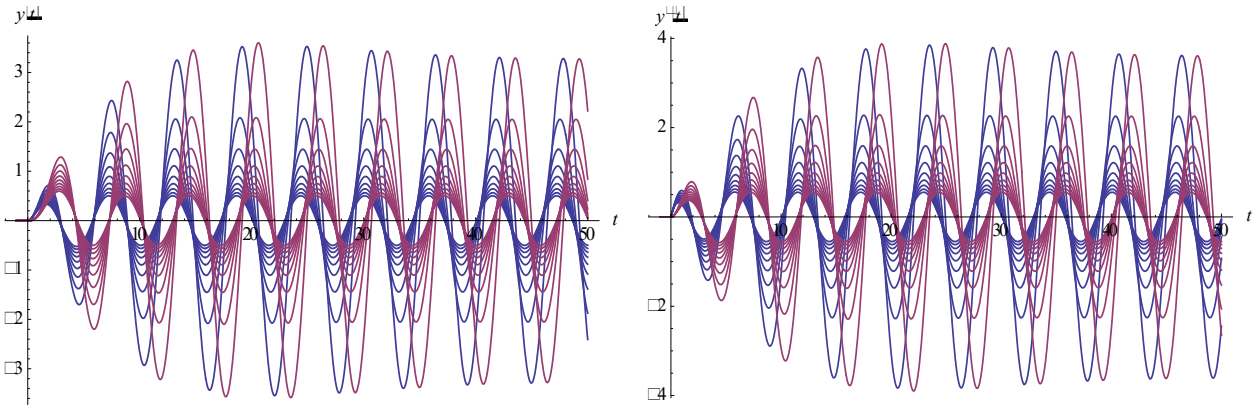

Figure 11: Simulated step response of the coil current and its time-derivative for various values of the damping parameter γ. We assumed the following set of parameters for this simulation: $\phi = 0$, $\omega_n = 1$, $\omega = 1.1$, and $\gamma = \{0.1, 0.2, \ldots, 0.9\}$.

It is useful to rewrite the particular solution as the sum of asymptotic (steady-state) and transient terms:

$$y_d(t) = u(t)\frac{e^{i\phi}\left[e^{i\omega t} - \frac{(\alpha + i\omega + \gamma)}{2\alpha}e^{-(\gamma-\alpha)t} - \frac{(\alpha - i\omega - \gamma)}{2\alpha}e^{-(\gamma+\alpha)t}\right]}{\left[\left(\omega_n{}^2 - \omega^2\right) + 2i\gamma\omega\right]}$$

$$= \frac{u(t)e^{i\phi}}{\left[\left(\omega_n{}^2 - \omega^2\right) + 2i\gamma\omega\right]}\left[\underbrace{e^{i\omega t}}_{\text{Steady state}} + \underbrace{\frac{(\lambda_2 - i\omega)}{2\alpha}e^{\lambda_1 t} - \frac{(\lambda_1 - i\omega)}{2\alpha}e^{\lambda_2 t}}_{\text{Transient}}\right]$$

$$\dot{y}_d(t) = \frac{e^{i\phi}}{\left[\left(\omega_n{}^2 - \omega^2\right) + 2i\gamma\omega\right]}\left[i\omega e^{i\omega t} + \frac{\lambda_1(\lambda_2 - i\omega)}{2\alpha}e^{\lambda_1 t} - \frac{\lambda_2(\lambda_1 - i\omega)}{2\alpha}e^{\lambda_2 t}\right], \quad t \geq 0.$$

In the most general case both circularly polarized components must be included in the driving function, which should then be written as

$$f(t) = u(t)\cos\left(\omega t + \phi\right) = u(t)e^{i\phi}\left[\frac{e^{i\omega t} + e^{-i\omega t}}{2}\right].$$

The differential equation is linear, so the particular solution in this case can easily be found by superposition. It is given by $\left(y_{d1}(t) + y_{d2}(t)\right)/2$, where $y_{d1}(t)$ is the solution for one circularly polarized component that we found earlier, and $y_{d2}(t)$ is the solution for the other component. The latter can be obtained from the former through the substitutions $\omega \to -\omega$ and $\phi \to -\phi$.

In this case the particular solution is given by

$$y_d(t) = Au(t)\left[\underbrace{\cos\left(\omega t+\phi+\theta\right)}_{\text{Steady state}}+\underbrace{a_1 e^{\lambda_1 t}+a_2 e^{\lambda_2 t}}_{\text{Transient}}\right],$$

$$a_1 \equiv \frac{\lambda_2\cos\left(\phi+\theta\right)+\omega\sin\left(\phi+\theta\right)}{2\alpha},\quad a_2 \equiv -\frac{\lambda_1\cos\left(\phi+\theta\right)+\omega\sin\left(\phi+\theta\right)}{2\alpha}.$$

$$\dot{y}_d(t) = A\left[-\omega\sin\left(\omega t+\phi+\theta\right)+a_1\lambda_1 e^{\lambda_1 t}+a_2\lambda_2 e^{\lambda_2 t}\right],\quad t\geq 0.$$

It is easy to verify that these expressions predict $y_d(0)=\dot{y}_d(0)=0$. Here the sinusoidal steady-state transfer function is defined as $A\left(\omega\right)e^{i\theta(\omega)} \equiv \left[\left({\omega_n}^2-\omega^2\right)+2i\gamma\omega\right]^{-1}$. It has the form of a second-order resonant lowpass filter. This function reaches its maximum magnitude when $\omega=\omega_n$, and is given by

$$A\left(\omega_n\right)e^{i\theta(\omega_n)} = \frac{1}{2i\gamma\omega_n} = \frac{R_s}{i\sqrt{1+\frac{R_c}{R_s}}\left(\frac{R_c R_s}{Z_0}+Z_0\right)}.$$

In the over-coupled case this expression reduces to

$$A\left(\omega_n\right)e^{i\theta(\omega_n)} \approx \frac{R_s}{iZ_0\sqrt{1+\frac{R_c}{R_s}}}.$$

The resulting steady-state transfer function from input voltage to coil current is given by

$$TF\left(\omega_n\right) \equiv \left.\frac{I_c}{V_{in}}\right|_{ss} \approx \frac{1}{iZ_0\sqrt{1+\frac{R_c}{R_s}}} = \frac{1}{i\omega_n L}.$$

Here we have used the un-normalized value of ω_n for clarity. We see that the steady-state transfer function is simply the admittance of the coil at the input frequency. This result is identical to that obtained with an un-tuned coil. It again demonstrates the fact that over-coupled tuned probes are very similar to un-tuned probes.

General solution

The general solution to the driven differential equation is simply the sum of the homogeneous and particular solutions:

$$\begin{aligned} y(t) &= y_h(t)+y_d(t) \\ &= Au(t)\left[\underbrace{\cos\left(\omega t+\phi+\theta\right)}_{\text{Steady state}}+\underbrace{\left(a_1+c_1\right)a_1 e^{\lambda_1 t}+\left(a_2+c_2\right)e^{\lambda_2 t}}_{\text{Transient}}\right]. \end{aligned}$$

The driven solution must have $y_d(0) = 0$ and $\dot{y}_d(0) = 0$, so $y(0) = y_h(0)$ and $\dot{y}(0) = \dot{y}_h(0)$. Thus

$$\begin{bmatrix} c_1 \\ c_2 \end{bmatrix} = \begin{bmatrix} 1 & 1 \\ \lambda_1 & \lambda_2 \end{bmatrix}^{-1} \begin{bmatrix} y(0) \\ \dot{y}(0) \end{bmatrix} = \frac{1}{2\alpha} \begin{bmatrix} -\lambda_2 y(0) + \dot{y}(0) \\ \lambda_1 y(0) - \dot{y}(0) \end{bmatrix}.$$

Let's assume that the output has reached its steady-state value before the input phase changes from ϕ to ϕ' at time $t = T$. In this case the initial amplitudes of the transient components due to the homogeneous solution are c_1 and c_2, where the coefficients are given by:

$$\begin{aligned}
y_d(0) &= A\cos(\omega T + \phi + \theta) \\
\dot{y}_d(0) &= -A\omega\sin(\omega T + \phi + \theta) \\
\begin{bmatrix} c_1 \\ c_2 \end{bmatrix} &= A\begin{bmatrix} 1 & 1 \\ \lambda_1 & \lambda_2 \end{bmatrix}^{-1} \begin{bmatrix} \cos(\omega T + \phi + \theta) \\ -\omega\sin(\omega T + \phi + \theta) \end{bmatrix} = \frac{A}{\lambda_2 - \lambda_1} \begin{bmatrix} \lambda_2 & -1 \\ -\lambda_1 & 1 \end{bmatrix} \begin{bmatrix} \cos(\omega T + \phi + \theta) \\ -\omega\sin(\omega T + \phi + \theta) \end{bmatrix} \\
&= -\frac{A}{2\alpha} \begin{bmatrix} \lambda_2\cos(\omega T + \phi + \theta) + \omega\sin(\omega T + \phi + \theta) \\ -\lambda_1\cos(\omega T + \phi + \theta) - \omega\sin(\omega T + \phi + \theta) \end{bmatrix}.
\end{aligned}$$

Here we have used the fact that $\lambda_1 - \lambda_2 = 2\alpha$ to simplify the expression. The initial amplitudes of the transient components due to the particular solution are

$$\begin{bmatrix} a_1 \\ a_2 \end{bmatrix} = \frac{A}{2\alpha} \begin{bmatrix} \lambda_2\cos(\omega T + \phi' + \theta) + \omega\sin(\omega T + \phi' + \theta) \\ -\lambda_1\cos(\omega T + \phi' + \theta) - \omega\sin(\omega T + \phi' + \theta) \end{bmatrix}.$$

In order to cancel out the transients, we need to have

$$\begin{aligned}
&\begin{bmatrix} a_1 \\ a_2 \end{bmatrix} + \begin{bmatrix} c_1 \\ c_2 \end{bmatrix} = 0, \quad \text{which implies that:} \\
&\lambda_2\cos(\omega T + \phi' + \theta) + \omega\sin(\omega T + \phi' + \theta) = \lambda_2\cos(\omega T + \phi + \theta) + \omega\sin(\omega T + \phi + \theta) \\
&\lambda_1\cos(\omega T + \phi' + \theta) + \omega\sin(\omega T + \phi' + \theta) = \lambda_1\cos(\omega T + \phi + \theta) + \omega\sin(\omega T + \phi + \theta).
\end{aligned}$$

Unfortunately these equations have no general solutions apart from the trivial case of no phase change ($\phi' = \phi$). Unlike in the case of the un-tuned coil, there is therefore no general way to cancel the transients produced by a phase-modulated RF pulse.

However, these conditions are simplified in the over-coupled case, i.e., when $\gamma \gg 1$. In this case $\lambda_1 \approx 0$ and $\lambda_2 \approx -2\gamma$, resulting in

$$\begin{aligned}
-2\gamma\cos(\omega T + \phi' + \theta) + \omega\sin(\omega T + \phi' + \theta) &= -2\gamma\cos(\omega T + \phi + \theta) + \omega\sin(\omega T + \phi + \theta) \\
\omega\sin(\omega T + \phi' + \theta) &= \omega\sin(\omega T + \phi + \theta).
\end{aligned}$$

The second condition can be ignored if the operating frequency $\omega \approx 1$, which is typical. In this case $\gamma \gg \omega$ and the transient elimination condition reduces to $\cos(\omega T + \phi' + \theta) = \cos(\omega T + \phi + \theta)$, which is identical to that of an un-tuned coil. This result again demonstrates that an over-coupled tuned probe is very similar to an un-tuned probe.

Finally, the calculated coil current must be converted to the rotating frame for spin dynamics simulations. The conversion process is identical to that described for un-tuned probes.

Receiver dynamics

We consider the situation after the probe and receiver have recovered from the effects of an RF pulse. The effects of any probe on the induced NMR signal v_{nmr} can then be expressed as a linear time-invariant (LTI) filter $G_R(\omega) \equiv S(\omega) / S_c(\omega)$. Here $S_c(\omega)$ and $S(\omega)$ are the spectra of v_{nmr} (signal induced on the coil) and v_{rx} (signal across the receiver input terminals), respectively. Our model of the probe in receive mode is shown in Figure 12.

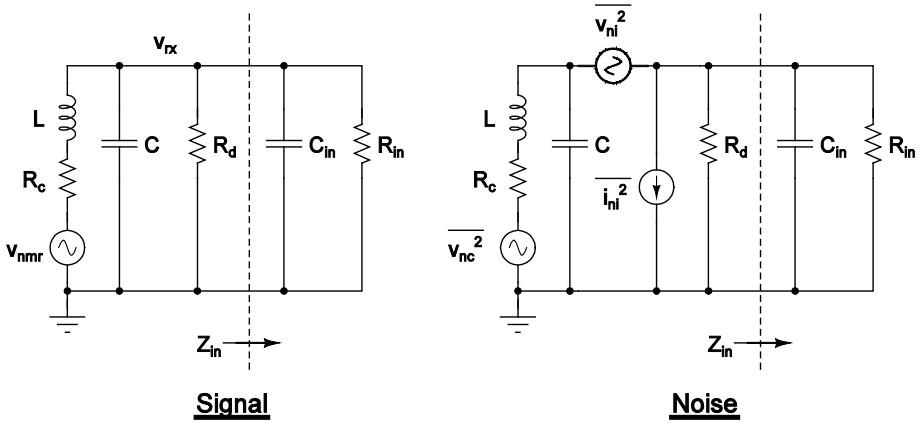

Figure 12: Model of a tuned NMR probe during receive mode for calculating signal (left) and noise (right) transfer functions.

In the case of a simple tuned probe, circuit analysis shows that

$$G_R(\omega) = \frac{1}{1 + (i\omega L + R_c)(i\omega C + G_d + Y_{in})}.$$

Here $G_d = 1/R_d$ denotes the conductance of any damping resistor present across the probe, while $Y_{in} = 1/Z_{in}$ is the input admittance of the receiver. At typical NMR frequencies most receivers have an input admittance that is well-modeled by a parallel RC circuit, resulting in $Y_{in} = i\omega C_{in} + G_{in}$. In this case the receiver transfer function is given by

$$G_R(\omega) = \frac{1}{(i\omega)^2 L(C + C_{in}) + i\omega\left[L(G_d + G_{in}) + R_c(C + C_{in})\right] + \left[1 + R_c(G_d + G_{in})\right]}.$$

This expression can be rewritten in standard form as

$$G_R(\omega) \equiv \frac{A_0}{(i\omega)^2 \tau^2 + i\omega(\tau/Q) + 1} = \frac{A_0}{(1-\omega^2\tau^2) + i(\omega\tau/Q)}.$$

The standard form shown above is the transfer function of a second-order resonant low-pass filter. Here $A_0 = \frac{1}{1 + R_c(G_d + G_{in})}$ is the DC gain of the filter, $\tau = \sqrt{A_0 L(C + C_{in})}$ is its natural time constant, and $Q = \frac{\tau}{L(G_d + G_{in}) + R_c(C + C_{in})}$ is its quality factor. The natural resonant frequency and 3 dB bandwidth of the filter are $\omega_n = 1/\tau$ and ω_n / Q, respectively. This frequency also results in the largest signal gain, given by $|G_R(\omega_n)| = A_0 Q$, and a phase shift of $\pi/2$ through the probe.

In most practical low-frequency NMR systems the input impedance of the receiver is much larger than that of the probe ($C_{in} \ll C$ and $G_{in} R_c \ll 1$), so these expressions simplify to $A_0 \approx \frac{1}{1 + R_c G_d} \approx 1$, $\tau = \sqrt{LC}$, and $Q \approx \frac{Z_0}{R_c + Z_0^2 / R_d} = \frac{Q_0}{1 + Q_0(Z_0 / R_d)}$. Here $Z_0 = \sqrt{L/C}$ is the characteristic impedance of the probe, and $Q_0 = Z_0 / R_c$ is the quality factor of the coil.

The phase of the receiver transfer function can be written as

$$\phi = -\tan^{-1}\left(\frac{\omega\tau/Q}{1-\omega^2\tau^2}\right),$$

which starts from 0 at DC, reaches $-\pi/2$ at resonance ($\omega\tau = 1$), and ends at $-\pi$ at high frequencies. The resultant group delay is given by

$$\tau_g = \frac{d\phi}{d\omega} = \left(\frac{\tau}{Q}\right)\frac{1+\omega^2\tau^2}{(1-\omega^2\tau^2)^2 + (\omega\tau/Q)^2} = \left(\frac{\tau}{QA_0^2}\right)|G_R(\omega)|^2 (1+\omega^2\tau^2).$$

Near resonance ($\omega\tau = 1$) we can write

$$\tau_g \approx \left(\frac{2\tau}{QA_0^2}\right)|G_R(\omega)|^2.$$

Thus the group delay of the tuned receiver is proportional to the square of the signal gain as a function of frequency. It is maximized exactly at resonance, where it is equal to

$$\tau_{g0} \equiv \left.\frac{d\phi}{d\omega}\right|_{\omega\tau=1} = \left(\frac{\tau}{Q}\right)2Q^2 = 2Q\tau.$$

Very close to resonance, we can write $\omega\tau \equiv 1+\Delta$, where $|\Delta| \ll 1$. In this case the phase of the transfer can be linearized, resulting in constant group delay equal to τ_{g0}:

$$\phi = -\left(\frac{\pi}{2} + \tan^{-1}(2Q\Delta)\right) \approx -\left(\frac{\pi}{2} + 2Q\Delta\right), \quad \Delta \ll \frac{1}{2Q}.$$

The group delay of the receiver decreases to $\tau_{g0}/2$ when the signal gain decreases by 3 dB, resulting in an average delay of approximately $0.75\tau_{g0}$ over its 3 dB bandwidth.

In order to provide the maximum voltage gain for on-resonance NMR signals we usually tune the probe, i.e., ensure that $\omega_0\tau = 1$, where ω_0 is the nominal Larmor frequency. In this case the received NMR echoes will be time-delayed by an amount $\tau_g = \beta\tau_{g0}$, where $0 < \beta < 1$ is a constant. The value of β depends on the bandwidth of the echoes relative to the probe. It increases as the relative echo bandwidth decreases, and approaches 1 when the echoes become much more narrowband than the probe.

The resulting time delay can be significant for high-*Q* probes at low Larmor frequencies. In general, such *Q*-dependent delays introduce an imaginary component to the echo spectrum that is anti-symmetric about $\Delta\omega_0 = 0$, and therefore not removable by simple phase rotation of the echo. A frequency-dependent phase correction $\exp\left(i\tau_g\Delta\omega_0\right)$ can be applied to the spectrum of each acquired echo to reduce this effect during simulations. Here τ_g is the signal delay and $\Delta\omega_0 \equiv \omega - \omega_0$ is the resonance offset frequency. Typically we implement a so-called "first-order" phase correction by keeping τ_g fixed at $\overline{\tau_g}$, its average value over the signal bandwidth. During experiments the same correction can be implemented by shifting the acquisition window by the amount $\overline{\tau_g}$. However, since the actual signal delay varies with $\Delta\omega_0$, no first-order correction can *completely* remove the imaginary component over the entire signal bandwidth. Thus, tuned receivers always distort the shape of time-domain echoes in addition to delaying them.

Noise and signal detection

The normal output of an NMR measurement is a single complex number per spin echo. This is known as the echo amplitude. The ratio between the mean echo amplitude and its standard deviation defines the signal-to-noise ratio (SNR) of the measurement. In this section we describe how to calculate the SNR.

Noise model

Winding resistance in the coil and conductive losses in the sample both generate thermal noise. Such noise sources can be assumed to be frequency-independent or white over the bandwidth of interest (usually no larger than $\pm 5\omega_1$ around the Larmor frequency). Their combined effects can be modeled by

an effective resistance R_c in series with the coil. The power spectral density (PSD) of the noise voltage $\overline{v_{nc}^2}$ generated by R_c is given by $N_0 = 4kTR_c$.

The noise generated by R_c (''probe noise'') has exactly the same transfer function $G_R(\omega)$ to the receiver input as the NMR signal. In general $|G_R(\omega)|$ varies with frequency, so the receiver sees colored probe noise with a frequency-dependent PSD $N_0|G_R(\omega)|^2$. The total noise seen by the receiver is the sum of this component and the receiver's own input-referred noise. The latter is usually modeled by two noise sources: a voltage source $\overline{v_{ni}^2}$ in series with the input ("receiver voltage noise"), and a current source $\overline{i_{ni}^2}$ in parallel with the input ("receiver current noise"), as shown in Figure 12.

The total voltage noise PSD at the receiver input terminals is then given by

$$N(\omega) = \underbrace{N_0|G_R(\omega)|^2}_{\text{Colored noise from probe}} + \underbrace{V_{ni}^2(\omega)}_{\text{Voltage noise from receiver}} + \underbrace{I_{ni}^2(\omega)|Z_s(\omega)|^2}_{\text{Current noise from receiver}}.$$

Here $V_{ni}^2(\omega)$ and $I_{ni}^2(\omega)$ are the PSDs of the receiver voltage and current noise sources, respectively, and $Z_s(\omega)$ is the effective impedance across the receiver terminals. The latter is defined as $Z_s = Z_p \,||\, Z_{in}$, where Z_p is the impedance seen by looking into the probe and Z_{in} is the input impedance of the receiver.

The noise figure (NF) of the receiver is defined as the ratio of input and output SNR, and should be as close to 1 (0 dB) as possible. In our case it is given by

$$\begin{aligned} NF(\omega) &= \frac{\left(S_c(\omega)/N_0\right)}{\left(S_c(\omega)|G_R(\omega)|^2/N(\omega)\right)} = \frac{N(\omega)}{N_0|G_R(\omega)|^2} \\ &= \frac{N_0|G_R(\omega)|^2 + V_{ni}^2(\omega) + I_{ni}^2(\omega)|Z_s(\omega)|^2}{N_0|G_R(\omega)|^2} \\ &= 1 + \frac{V_{ni}^2(\omega) + I_{ni}^2(\omega)|Z_s(\omega)|^2}{N_0|G_R(\omega)|^2}. \end{aligned}$$

Here $S_c(\omega)$ is the spectrum of the NMR signal induced on the coil.

Signal detection

The optimum signal detector in the presence of additive, white, Gaussian noise (AWGN) is the matched filter. This can take the form of a linear time-invariant (LTI) filter that is applied to real-time (streaming) data, or a "window" function that is applied to recorded data.

In real life, signal acquisition only occurs over a finite time window $w(t)$. This fact can be modeled by multiplying the time-domain signal $s(t)$ seen by the receiver with the window $w(t)$, or by convolving the frequency-domain signal with its spectrum $W(\omega)$:

$$s_a(t) \equiv s(t)w(t),$$
$$S_a(\omega) = S(\omega) * W(\omega).$$

Since $w(t)$ is generally longer than $s(t)$ (in order to acquire all of it), $W(\omega)$ is narrower than $S(\omega) = S_c(\omega)G_R(\omega)$. Hence the main effect of windowing is to remove fine spectral features (narrower than $W(\omega)$) from the acquired spectrum $S_a(\omega)$, which therefore looks like a "blurred'' version of $S(\omega)$.

The output of the filter, which is assumed to have an impulse response *h*(*t*), is given by

$$y(t) = \int_{-T_a/2}^{T_a/2} s(\tau)h(t-\tau)d\tau$$
$$= \int_{-\infty}^{\infty} s_a(\tau)h(t-\tau)d\tau \equiv s_a(t) * h(t).$$

In order to maximize SNR at a particular time (say *t* = 0), the matched filter must have an impulse response that is a time-reversed version of $s_a^*(t)$, i.e., $h_M(t) = s_a^*(-t)$. Here $s_a^*(t)$ is the complex conjugate of the signal that we expect to acquire. The expected signal is known as the "symbol" in communication theory. It is assumed to be known *a priori* – in our case, through spin dynamics calculations and circuit simulations.

The output at *t* = 0 after matched filtering is a single real number s_M, which is then given by

$$y_M(t) = \int_{-\infty}^{\infty} s_a(\tau)s_a^*(\tau - t)d\tau$$
$$s_M \equiv y_M(0) = \int_{-\infty}^{\infty} s_a(\tau)s_a^*(\tau)d\tau = \int_{-\infty}^{\infty} |s_a(\tau)|^2 d\tau$$

An equivalent computation can be performed in the frequency domain. Using the properties of Fourier transforms, we have $H_M(\omega) = \alpha S_a^*(\omega)$. In addition, the convolution is replaced by a simple multiplication (windowing operation), resulting in

$$Y_M(\omega) = S_a(\omega)H_M(\omega) = |S_a(\omega)|^2$$
$$s_M = y_M(0) = \int_{-\infty}^{\infty} Y_M(\omega)d\omega = \int_{-\infty}^{\infty} |S_a(\omega)|^2 d\omega$$

The detected noise variance is given by

$$Y_N{}^2(\omega) = N_0 \left|H_M(\omega)\right|^2 = N_0 \left|S_a(\omega)\right|^2$$
$$\sigma^2 = \int_{-\infty}^{\infty} Y_N{}^2(\omega) d\omega = N_0 \int_{-\infty}^{\infty} \left|S_a(\omega)\right|^2 d\omega.$$

Here N_0 is the power spectral density (PSD) of the AWGN present at the detector input. The output SNR (in voltage units) is therefore given by

$$SNR = \frac{S_M}{\sigma} = \frac{\int_{-\infty}^{\infty} \left|S_a(\omega)\right|^2 d\omega}{\sqrt{N_0 \int_{-\infty}^{\infty} \left|S_a(\omega)\right|^2 d\omega}} = \sqrt{\frac{1}{N_0} \int_{-\infty}^{\infty} \left|S_a(\omega)\right|^2 d\omega}.$$

Using Parseval's theorem, this expression can also be written as

$$SNR = \sqrt{\frac{1}{N_0} \int_{-\infty}^{\infty} \left|s_a(t)\right|^2 dt} = \sqrt{\frac{1}{N_0} \int_{-T_{acq}/2}^{T_{acq}/2} \left|s(t)\right|^2 dt}.$$

This equation shows that the output SNR increases monotonically as T_{acq} increases, i.e., the acquisition window becomes longer, and asymptotes to a maximum value when it becomes much longer than the duration of the signal. This behavior *only* occurs when we use a matched filter to process the signal. When other filter shapes are used the output SNR typically increases with T_{acq}, reaches a maximum at some finite value, and then decreases.

The theory described above cannot be directly applied to narrowband NMR probes, since they do not exhibit white Gaussian noise. In general, the noise is "colored", i.e., its spectrum is not flat. However, the matched filter can be modified to account for this fact. It can be shown that the new optimum solution is to use an additional ''whitening'' filter $H_w(\omega)$ in front of the usual matched filter $H_M(\omega)$. The job of the pre-whitening filter is to convert the colored noise PSD $N(\omega)$ into white noise. The "whitened" signal can now be filtered by $H_M(\omega)$ in the usual way.

It is easy to see that the whitening filter must therefore be defined as

$$H_W(\omega) = \sqrt{\frac{N_{out}}{N(\omega)}},$$

where N_{out} is the constant (frequency-independent or white) noise PSD at the output of the filter. This filter may not be causal. However, NMR signal processing is usually performed on pre-recorded data, which makes it possible to implement even non-causal whitening filters.

After the whitening operation, the signal is given by $S_a(\omega)H_W(\omega)$, so the required matched filter is

$$H_M(\omega) \equiv \left[S_a(\omega)H_W(\omega)\right]^* = S_a{}^*(\omega)H_W{}^*(\omega)$$

The whitening and matched filters can now be combined into a single, modified matched filter that is given by

$$H_M'(\omega) \equiv H_W(\omega)H_M(\omega) = S_a^*(\omega)\left|H_W(\omega)\right|^2$$
$$= N_{out}\left(\frac{S_a^*(\omega)}{N(\omega)}\right)$$

The detected signal amplitude is now given by

$$Y_M(\omega) = S_a(\omega)H_M'(\omega) = \frac{N_{out}\left|S_a(\omega)\right|^2}{N(\omega)}$$
$$s_M = \int_{-\infty}^{\infty} Y_M(\omega)d\omega = N_{out}\int_{-\infty}^{\infty}\frac{\left|S_a(\omega)\right|^2}{N(\omega)}d\omega = N_{out}\int_{-\infty}^{\infty}\left|SNR(\omega)\right|^2 d\omega$$

The optimally-detected signal amplitude is purely real, and is proportional to the integral of the expected signal-to-noise ratio (SNR) in power units as a function of frequency. This result makes intuitive sense. It is a generalization of our earlier result for white noise. In that case SNR was simply proportional to the PSD of the signal, since the PSD of the noise was defined to be constant.

Similarly, the detected noise variance is given by

$$Y_N^2(\omega) = N(\omega)\left|H_M'(\omega)\right|^2 = N(\omega)\left|S_a(\omega)\right|^2\left|H_W(\omega)\right|^4 = N_{out}^2\frac{\left|S_a(\omega)\right|^2}{N(\omega)}$$
$$\sigma^2 = \int_{-\infty}^{\infty} Y_N^2(\omega)d\omega = N_{out}^2\int_{-\infty}^{\infty}\frac{\left|S_a(\omega)\right|^2}{N(\omega)}d\omega.$$

The output SNR (in voltage units) is therefore given by

$$SNR = \frac{s_M}{\sigma} = \frac{N_{out}\int_{-\infty}^{\infty}\frac{\left|S_a(\omega)\right|^2}{N(\omega)}d\omega}{\sqrt{N_{out}^2\int_{-\infty}^{\infty}\frac{\left|S_a(\omega)\right|^2}{N(\omega)}d\omega}} = \sqrt{\int_{-\infty}^{\infty}\frac{\left|S_a(\omega)\right|^2}{N(\omega)}d\omega} = \sqrt{\int_{-\infty}^{\infty}\left|SNR(\omega)\right|^2 d\omega}.$$

Treating the SNR spectrum as a signal and applying Parseval's theorem to it, we can formally rewrite this expression as $SNR = \sqrt{\int_{-\infty}^{\infty}\left|snr(t)\right|^2 dt}$, where *snr*(*t*) is the "time-domain SNR function". It is clear that this function must be zero outside the acquisition window (where there is no signal), so we can write

$$SNR = \sqrt{\int_{-T_{acq}/2}^{T_{acq}/2}\left|snr(t)\right|^2 dt}.$$

This equation shows that the output SNR with a matched filter increases monotonically as T_{acq} increases. It generalizes our earlier result, which was derived for the special case of white noise.

Let us consider the example of a receiver with low noise figure, i.e., one in which the total input noise is dominated by probe noise. In this case $N(\omega) \approx N_0 \left|G_R(\omega)\right|^2$, so the optimum filter is given by

$$H_M'(\omega) = N_{out}\left(\frac{S_a^*(\omega)}{N(\omega)}\right) \approx N_{out}\frac{S_c^*(\omega)G_R^*(\omega)W(\omega)}{N_0\left|G_R(\omega)\right|^2} = \frac{N_{out}}{N_0}\left(\frac{S_c^*(\omega)W(\omega)}{G_R(\omega)}\right).$$

We see that the optimum filter is proportional to the windowed spectrum of the input signal divided by the probe gain. Many common pulse sequences produce NMR signal spectra that have maximum amplitudes at the Larmor frequency ω_0, while the probe is generally also tuned to have maximum gain at the same frequency. The two maxima have a tendency to cancel when one function is divided by the other, so $H_M'(\omega)$ often has a "flat" region around ω_0, as shown in Figure 13. Physically, this shape expresses the fact that the signal and noise spectra have similar shapes near ω_0, so the SNR tends to remain constant in this region.

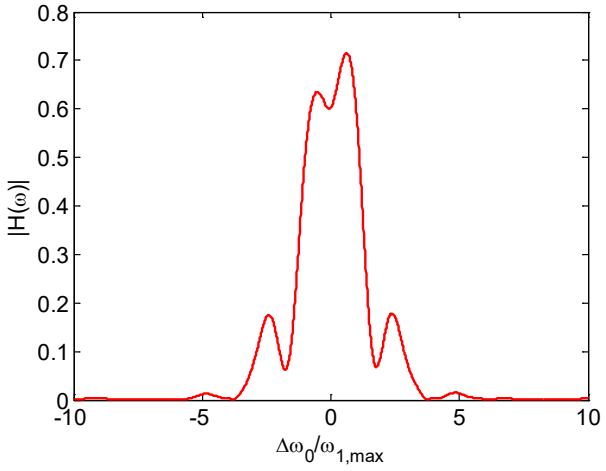

Figure 13: A typical matched filter for a CPMG pulse sequence at low Larmor frequencies. We assumed a tuned NMR probe, nominal Larmor frequency of $\omega_0 = 2\pi$ x 250 kHz, and a nutation frequency of $\omega_{1,max} = 2\pi$ x 12.5 kHz while creating this plot. We also assumed a constant field gradient and constant RF field strength. The NMR signal frequency is given by $\omega = \omega_0 + \Delta\omega_0$, where $\Delta\omega_0$ is the resonance offset frequency.

The effects of colored noise become important when the bandwidth of the probe is comparable or smaller than that of the signal, i.e., in narrowband probes where $BW_{probe} \leq BW_{signal}$. In such cases the noise PSD at the receiver varies significantly across the signal bandwidth. Such effects are important for high-Q probes at low Larmor frequencies (since $BW_{probe} \propto \omega_0 / Q$), and also when broadband pulse sequences increase the bandwidth of the NMR signal.

OCT pulses for tuned probes

In this section we describe the design of refocusing and excitation pulses for CPMG-type sequences that are optimized for tuned NMR probes. We will have to integrate our circuit models for the transmitter

and receiver into existing spin dynamics code for this process to work. This step is not necessary for un-tuned NMR probes, since we have shown that transient coil currents can be effectively canceled in this case. Given enough phase and timing resolution, phase-modulated pulse sequences for un-tuned probes can therefore be optimized purely at the spin dynamics level.

We simulate the NMR signal produced by a pulse sequence by calculating the independent evolution of a large number of isochromats that are distributed over the $(\Delta\omega_0, \omega_1)$ plane, where $\Delta\omega_0$ is the resonance offset frequency and $\omega_1 = B_1 / \gamma$ is the nutation frequency of the spins. In this report we will assume that $\Delta\omega_0$ has a uniform distribution over the range $\left[-\Delta\omega_{0,max}, \Delta\omega_{0,max}\right]$, and that ω_1 is constant. This situation, which corresponds to a constant B_0 gradient and no variation in B_1 over the sample, is a good first-order model of many NMR well-logging tools.

The asymptotic NMR signal induced on the coil by a CPMG sequence in the presence of a static field gradient can be written as [4]:

$$S_c(\Delta\omega_0) \propto (\omega_0 + \Delta\omega_0)^2 \left[m_{exc}(\Delta\omega_0) \cdot \hat{n}(\Delta\omega_0)\right] n_\perp(\Delta\omega_0)$$
$$\propto \omega_0^2 \left(1 + \frac{\Delta\omega_0}{\omega_0}\right)^2 \left[m_{exc}(\Delta\omega_0) \cdot \hat{n}(\Delta\omega_0)\right] n_\perp(\Delta\omega_0).$$

Here ω_0 is the average Larmor frequency (corresponding to $\Delta\omega_0 = 0$), m_{exc} is the magnetization produced by the excitation pulse, $\hat{n}$ is the effective rotation axis of the refocusing cycle, and $n_\perp = n_y + i n_x$ is the transverse component of $\hat{n}$. The initial term takes into account the fact that the induced signal amplitude is proportional to the square of the absolute frequency $(\omega_0 + \Delta\omega_0)$. One factor of $(\omega_0 + \Delta\omega_0)$ arises from thermal polarization via the Boltzmann relationship, while another arises from the fact that the coil detects the rate of change of magnetic flux, not the flux itself. This term can be neglected during pulse optimization if $\Delta\omega_{0,\max} \ll \omega_0$, when the average Larmor frequency is much larger than the range of frequencies being simulated. We are, however, interested in relatively low Larmor frequencies, and therefore retain it.

We performed pulse optimizations at two nominal Larmor frequencies (250 kHz and 500 kHz) for a typical tuned NMR probe with actively damped receiver. We assumed the following parameter values for the system, unless otherwise specified:

Parameter	**Value at 250 kHz**	**Value at 500 kHz**	**Notes**
Coil inductance, *L*	15 μH	7.5 μH	
Coil series resistance, R_c	0.4 Ω	0.4 Ω	Coil *Q* = 59
Tuning capacitor, *C*	27 nF	13.5 nF	Resonant frequency = 250 kHz or 500 kHz, Z_0 = 23.6 Ω
Transmitter "on" resistance, $R_{s,on}$	5 Ω	5 Ω	Typical switch-based transmitter with step-up transformer

Transmitter "off" resistance, $R_{s,on}$	5 Ω	5 Ω	Q-switch "on" resistance
Transmitter timing steps per RF cycle, N	16	8	All pulse segment lengths quantized to 0.25 μs
T_{90} (rectangular pulse)	20 μs	20 μs	$\omega_{1,max}$ = 2π x 12.5 kHz
T_E (echo period)	280 μs	280 μs	7 x T_{180} = 14 x T_{90}
T_{acq} (acquisition window length)	160 μs	160 μs	4 x T_{180} = 8 x T_{90}
Receiver damping resistance, R_d	700 Ω	700 Ω	Damped Q = 19.7 (active damping, R_d assumed to be noiseless)
Receiver input impedance, Z_{in}	1 MΩ || 10 pF	1 MΩ || 10 pF	High input impedance preamplifier
Receiver voltage noise, v_{ni}	0.5 nV/Hz$^{1/2}$	0.5 nV/Hz$^{1/2}$	
Receiver voltage noise, i_{ni}	0.1 pA/Hz$^{1/2}$	0.1 pA/Hz$^{1/2}$	Noise match resistance, R_n = 5 kΩ
Matched filter type	Optimum, $H_M'(\omega)$	Optimum, $H_M'(\omega)$	Code allows other matched filters to be used instead
Simulation frequency range, $\pm\Delta\omega_{0,max}$	$10\omega_{1,max}$	$10\omega_{1,max}$	± 2π x 125 kHz around the nominal frequency in both cases

This acquisition window was chosen to be long enough to acquire essentially all the energy in the asymptotic echo. The Q of the receiver using active damping is given by

$$Q_d = \frac{R_d \,||\left(Q^2 R_c\right)}{Z_0}.$$

Here Q is the (un-damped) quality factor of the coil. The receiver transfer functions and noise figures that result from these parameter choices are shown in Figure 14.

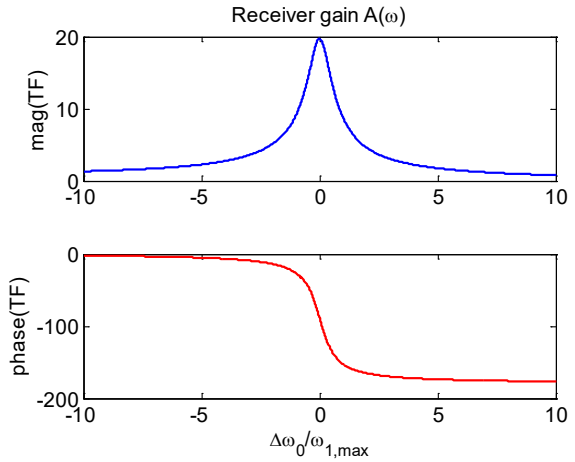

250 kHz

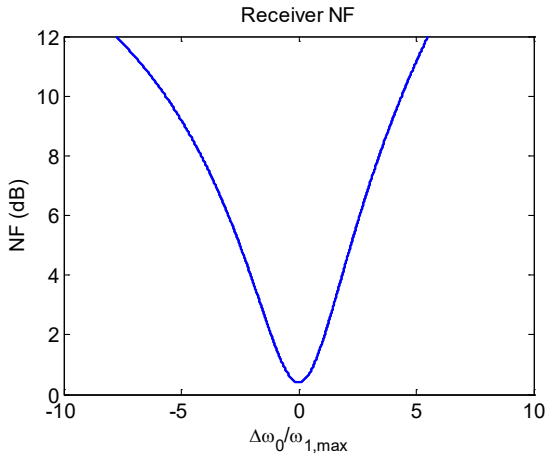

250 kHz

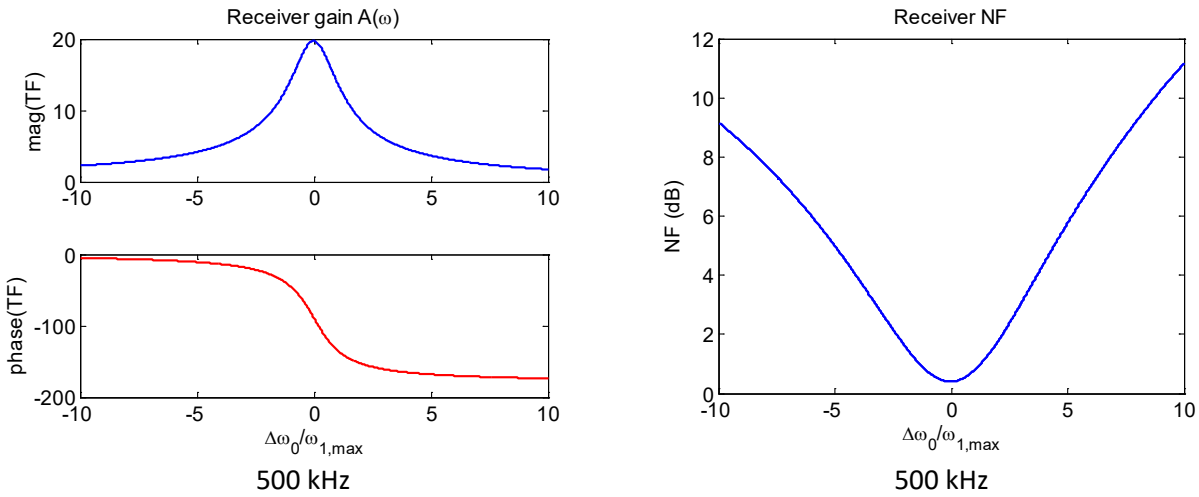

Figure 14: Simulated receiver transfer function (left) and noise figure (right) at two different Larmor frequencies for the parameter choices listed in the text. The damped *Q* of the receiver was Q_d = 19.7 in both cases.

We have calculated the asymptotic SNR produced by the default CPMG sequence (rectangular $\pi/2$ excitation pulse, rectangular π refocusing pulses) using the parameters listed above, but with different types of echo filtering. Matched filtering puts all the signal energy on the real channel (as shown earlier), so we only used the real part of the output of each filter to calculate the SNR. The results are plotted in Figure 15 as a function of the damped *Q* of the receiver for a nominal Larmor frequency of 250 kHz and three types of echo filter:

1. Simple integration, i.e., the filter value is kept constant during acquisition. The resulting time-domain window is rectangular, and corresponds to a sinc filter in the frequency domain. For this set of parameters we found that the SNR was maximized when T_{acq} = 2 x T_{180}, so we assumed this value while creating the plot.
2. Same as the previous case, but with a first order offset-frequency-dependent phase correction of $\exp\left(i\overline{\tau_g}\Delta\omega_0\right)$ applied to the echo spectrum to compensate for receiver group delay. We used $\overline{\tau_g} = 0.6\tau_{g0} = 1.2\left(Q_d / \omega_0\right)$, which for this set of parameters was found to minimize signal energy in the imaginary channel.
3. The optimum filter for white noise, assuming T_{acq} = 4 x T_{180}.
4. The actual optimum filter (which takes colored noise into account), assuming T_{acq} = 4 x T_{180}.

Figure 15 shows that substantial improvements in SNR are possible by using the optimum filter. The advantage increases with Q_d. This is because the total receiver noise becomes more and more "non-white" as Q_d increases. In addition, the SNR decreases for low values of Q_d irrespective of the type of filter. This is because the noise figure (NF) of the receiver increases as Q_d decreases. However, high values of receiver Q are associated with other problems, such as increased receiver settling time following a pulse, more sensitivity to salinity changes, etc. For our current choice of parameters $Q_d \approx 20$ appears to be an acceptable compromise between these conflicting factors.

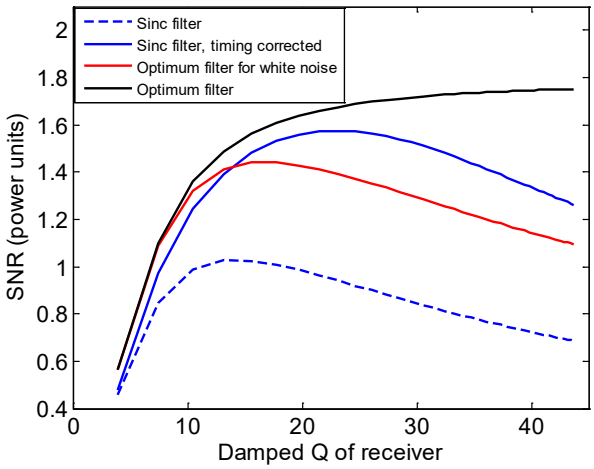

Figure 15: Calculated output SNR (in power units) of the default CPMG sequence at 250 kHz as a function of the damped *Q* of the receiver. The figure shows the SNR for three types of echo filtering: sinc filter (constant in time), optimum filter for white noise, and the actual optimum filter (taking colored noise into account). It also shows the SNR when a first-order frequency-dependent phase correction is applied before the sinc filter to compensate for receiver group delay.

In addition, we see that the SNR with simple integration is substantially increased if we compensate for receiver group delay by applying first-order frequency-dependent phase correction to the echo spectrum. This correction largely eliminates the anti-symmetric imaginary component of the echo, and transfers the corresponding energy to the real channel where it can contribute to the SNR. It is not necessary if we use a matched filter.

Refocusing pulse design

An ideal excitation pulse produces magnetization that is aligned with $\hat{n}$, i.e., $m_{exc}(\Delta\omega_0) = M_0\hat{n}(\Delta\omega_0)$ for all offsets $\Delta\omega_0$, where $M_0\hat{z}$ is the initial magnetization. In this case the asymptotic signal induced on the coil is maximized, and is given by

$$\begin{aligned} S_{c,\max}(\Delta\omega_0) &\propto (\omega_0+\Delta\omega_0)^2\left[\hat{n}(\Delta\omega_0)\cdot\hat{n}(\Delta\omega_0)\right]n_\perp(\Delta\omega_0) \\ &\propto (\omega_0+\Delta\omega_0)^2\left|\hat{n}(\Delta\omega_0)\right|^2 n_\perp(\Delta\omega_0) \\ &\propto (\omega_0+\Delta\omega_0)^2 n_\perp(\Delta\omega_0). \end{aligned}$$

We have used the fact that $\hat{n}$ is a refocusing axis and therefore must have $|\hat{n}|=1$ by definition. The resultant SNR after filtering by the receiver and optimum signal detection is given by

$$SNR_{\max} = \sqrt{\int_{-\infty}^{\infty}\frac{\left|S_{a,\max}(\omega)\right|^2}{N(\omega)}d\omega},$$

where $S_{a,\max}(\omega) = \left[S_{c,\max}(\omega) G_R(\omega)\right] * W(\omega)$ and $N(\omega) = N_0 \left|G_R(\omega)\right|^2 + V_{ni}^2(\omega) + I_{ni}^2(\omega)\left|Z_S(\omega)\right|^2$, as discussed earlier. This expression denotes the maximum SNR possible with a given refocusing cycle. We used it as the cost function while searching for refocusing pulses.

Our optimization procedure is shown in Figure 16. It is currently implemented in MATLAB. The cost function is calculated in several steps. First the coil current is calculated as a function of time, given the pulse parameters, by using the analytical solution described earlier. It is then converted to the rotating frame and quantized in steps of $1/(2\omega_0)$ to eliminate the counter-rotating component. The result is scaled by the specified coil sensitivity and fed into a general-purpose spin dynamics simulator. This block models the evolution of the spins as a series of offset-frequency-dependent rotations. The resultant asymptotic magnetization is filtered by the LTI receiver model to find the received signal, as described earlier. This model also includes a calculation of the received noise and SNR. These quantities are used to calculate the cost function. Finally, a general-purpose gradient-based constrained minimization algorithm (*fmincon*) is used to minimize the cost function. The latter is available as a standard function within the MATLAB Optimization Toolbox.

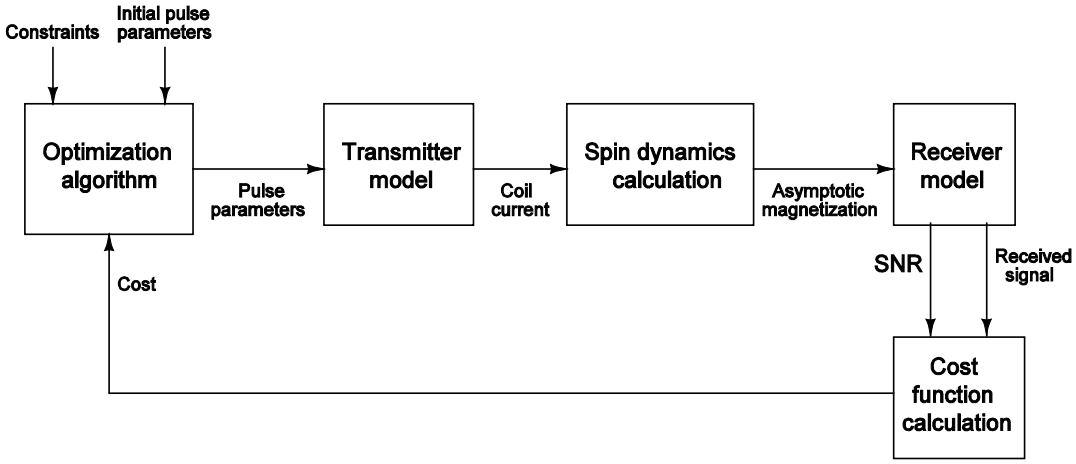

Figure 16: Schematic of the pulse optimization procedure. It is currently implemented in MATLAB.

We also assumed the following parameter values, based on prior experience, for the refocusing pulse to be optimized. These values were the same at both Larmor frequencies. No attempt was made to eliminate coil current transients.

Parameter	Value	Notes
Number of segments, N_{seg}	10	Constant amplitude, arbitrary phase
Segment length, T_{seg}	4 µs	$T_{seg} = T_{180}/10$
Total pulse length, $N_{seg}T_{seg}$	40 µs	Same as a rectangular 180 degree pulse

We found that the optimization landscape was highly non-convex, with many local optima for the algorithm to get stuck in. This is typical of NMR pulse design problems. We ran the optimization procedure several times with random initial conditions in order to overcome this problem. However, the

available SNR of the different solutions varied over a very narrow range (standard deviation ~1%), which indicates that the various local minima have similar depths. The best solutions at 250 kHz and 500 kHz are shown in Figure 17. The optimized phase profile is a smooth function in both cases.

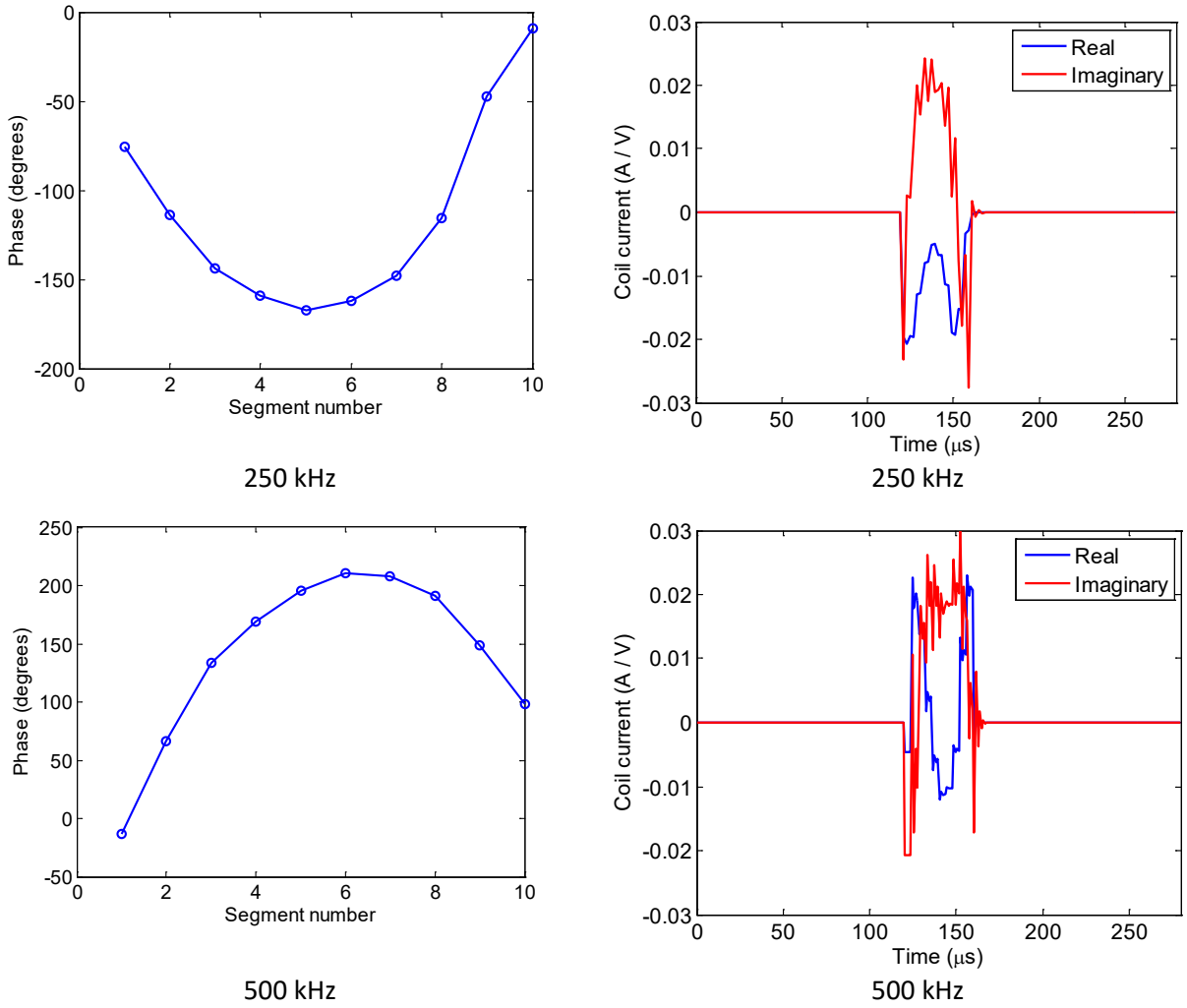

Figure 17: Segment phases (left) and simulated coil current in the rotating frame (right) for the optimized refocusing pulses described in the text.

The available SNR of our OCT refocusing pulses is compared to the default rectangular 180 degree (π) refocusing pulse in the table below. The results have been normalized to the SNR of the default CPMG sequence with rectangular 90 degree ($\pi/2$) excitation pulses and rectangular π excitation pulses at 250 kHz. We see that the OCT pulses can provide significantly more SNR.

It should be noted that the numbers in the table correspond to the SNR available from a perfectly axis-matched excitation pulse. The rectangular π pulse also has an available SNR that is significantly greater than 1, so we conclude that the rectangular $\pi/2$ excitation pulse is poorly axis-matched to it. In other words, the rectangular π pulse can also provide increased SNR if an appropriate excitation pulse is designed for it.

Larmor frequency	Refocusing pulse	Normalized available SNR (power units)
250 kHz	Rectangular, 180 degrees	1.434
250 kHz	OCT, 10 segments	1.967
500 kHz	Rectangular, 180 degrees	1.791
500 kHz	OCT, 10 segments	2.875

A perfectly axis-matched excitation pulse is needed to actually achieve the maximum SNR possible with a given refocusing pulse. We describe our search for such excitation pulses in the next section.

Excitation pulse design

We assumed the following parameter values, based on prior experience, for optimizing the excitation pulse. These values were the same at both Larmor frequencies. No attempt was made to eliminate coil current transients.

Parameter	Value	Notes
Number of segments, N_{seg}	80	Constant amplitude, arbitrary phase
Segment length, T_{seg}	4 µs	$T_{seg} = T_{180}/10$
Total pulse length, $N_{seg}T_{seg}$	320 µs	16 times longer than a rectangular 90 degree pulse

The overall optimization procedure was the same as shown in Figure 16. We optimized the axis-matched excitation pulse by maximizing the asymptotic SNR after matched filtering. We found that the optimization landscape was highly non-convex, with many local optima for the algorithm to get stuck in. This is typical of NMR pulse design problems. We ran the optimization procedure several times with random initial conditions in order to overcome this problem. The best solutions that we found at 250 kHz and 500 kHz are shown in Figure 18.

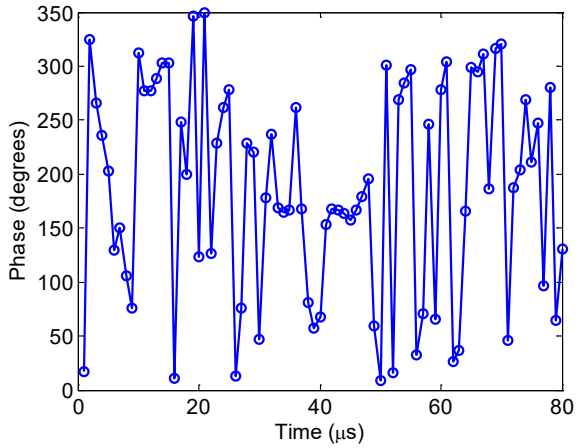

250 kHz

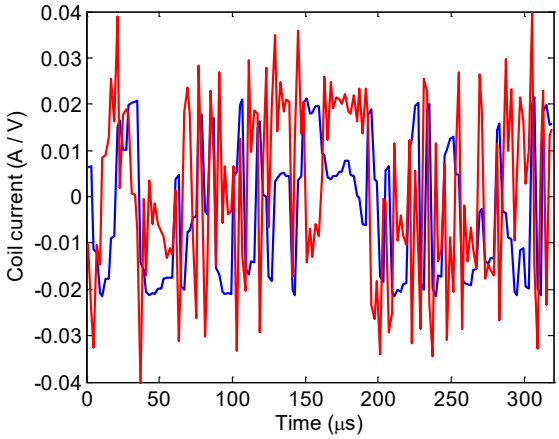

250 kHz

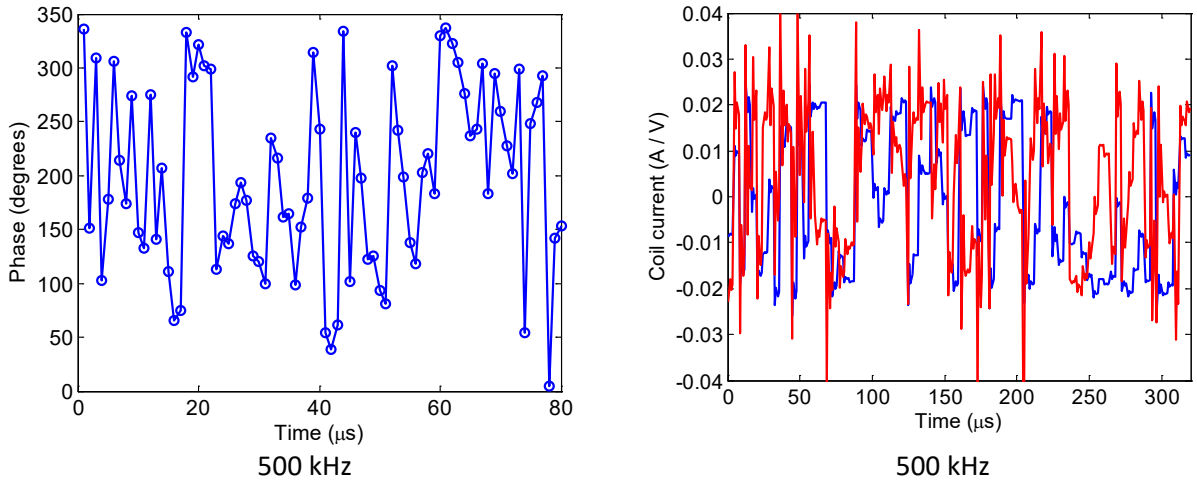

Figure 18: Segment phases (left) and simulated coil current in the rotating frame (right) for the optimized excitation pulses described in the text.

We can now create optimized CPMG sequences by combining an optimized refocusing pulse with the corresponding axis-matched excitation pulse. Figure 19 compares the performance of such OCT sequences and the standard rectangular $\pi/2$ – rectangular π CPMG sequence. For each sequence the figure shows the simulated asymptotic magnetization, receiver noise PSD, and optimum matched filter as a function of resonant offset frequency.

It is interesting to note that both OCT sequences produce their largest asymptotic magnetization at some positive offset frequency $\left(\Delta\omega_0 > 0\right)$. By contrast, the rectangular sequences produce their largest asymptotic magnetization at resonance $\left(\Delta\omega_0 = 0\right)$. This is because the optimizer recognized that greater SNR was available at positive offset frequencies. In fact, the amplitude of the induced NMR signal varies with offset frequency as $\left(\omega_0 + \Delta\omega_0\right)^2$, as explained earlier, while the noise figure of the tuned receiver is lowest at resonance. The optimizer trades off between these two frequency dependencies to maximize SNR, resulting in the observed frequency shift.

It should be noted that in real NMR systems more spins are often available at lower Larmor frequencies, which compensates for the reduced SNR *per spin* and therefore reduces or eliminates this effect. For example, in inside-out NMR systems such as well-logging tools, the static field gradient decreases as the distance *r* from the tool increases. In addition, the circumference of the excited region increases as $2\pi r$. As a result, the spin density along the offset frequency axis increases as the local Larmor frequency $\left(\omega_0 + \Delta\omega_0\right)$ decreases. We can account for this situation in our simulations by multiplying the asymptotic echo spectrum (before matched filtering) with a suitable frequency-dependent weighting function.

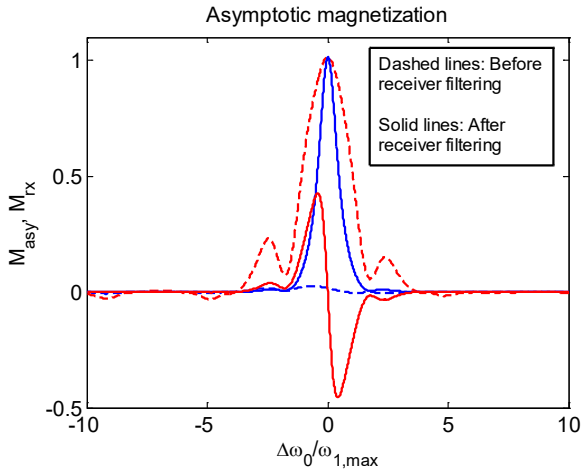

250 kHz, rectangular

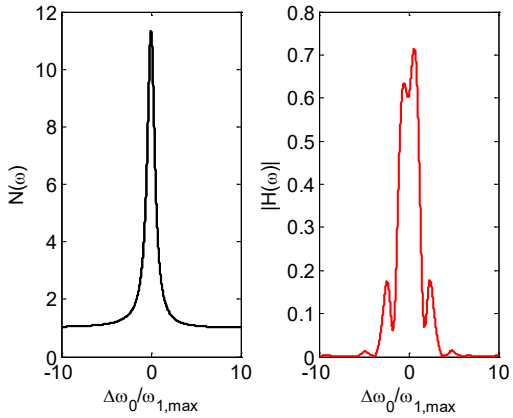

250 kHz, rectangular

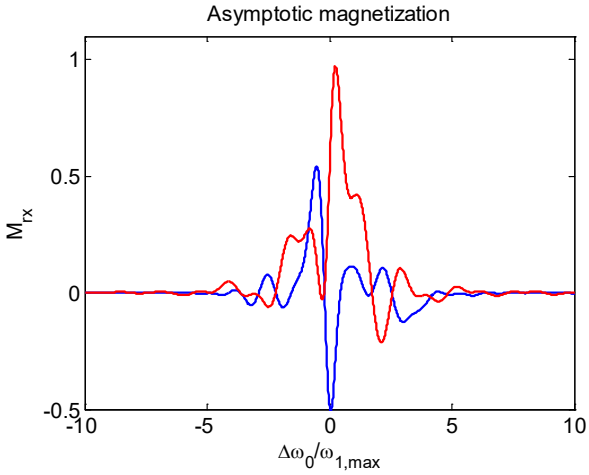

250 kHz, OCT

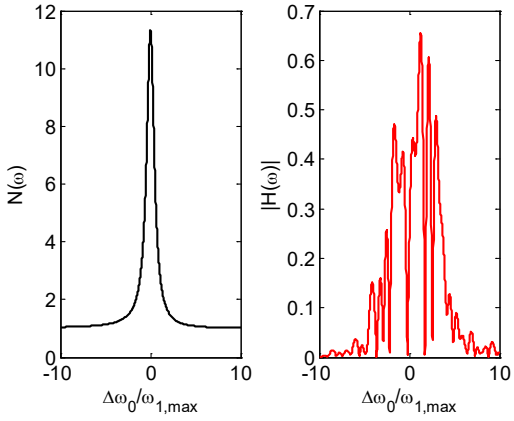

250 kHz, OCT

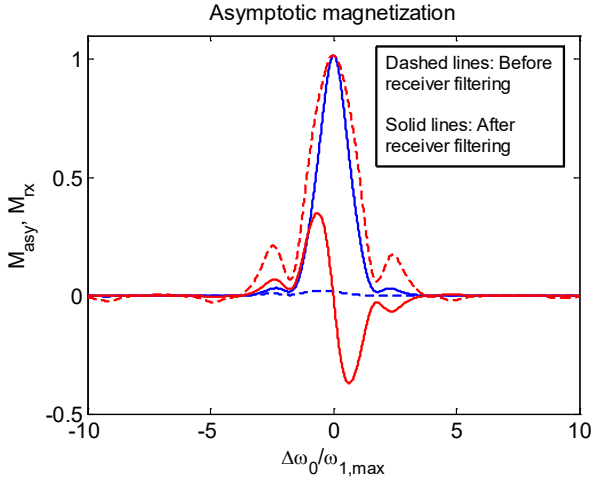

500 kHz, rectangular

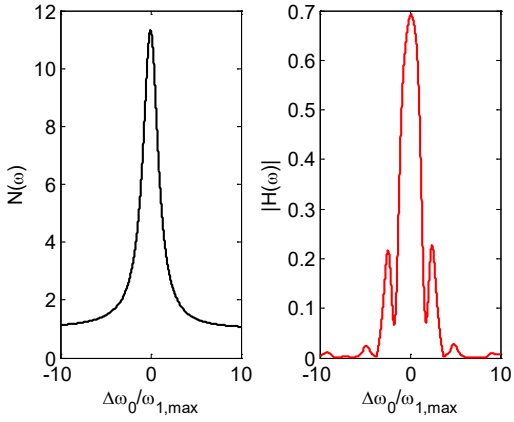

500 kHz, rectangular

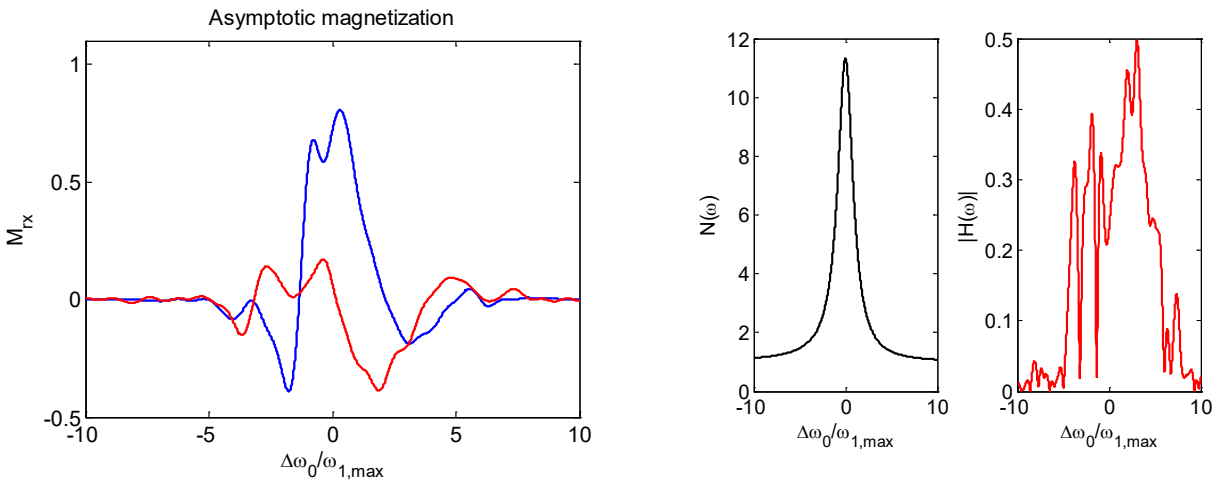

Figure 19: Asymptotic magnetization (left), receiver noise PSD and optimum matched filter (right) for the optimized and default CPMG sequences described in the text.

Phase cycling

An important practical concern with OCT sequences is their support of phase cycling, which is very useful for canceling probe ringing, detector offsets, etc. We have previously found that symmetric phase-alternating (SPA) refocusing pulses produce asymptotic magnetization that is symmetric about $\Delta\omega_0 = 0$ [2]. This allows a modified form of phase-cycling, known as phase-inversion, to be applied to the corresponding axis-matched excitation pulses. However, our current refocusing pulses are not of the SPA type, so phase-inversion does not work.

The simplest phase-cycling scheme for CPMG-type sequences is known as the phase-alternating pair (PAP). In this scheme the phase of the excitation pulse is shifted by π during every second scan. This shift inverts the asymptotic magnetization, thus allowing the phase cycle to be completed by subtracting the second scan from the first, non-inverted scan. We would like to implement a similar scheme for our OCT-based CPMG sequences. For this purpose we need excitation pulses that produce asymptotic magnetization that is precisely the inverse of that produced by our existing excitation pulses. The phases of such "inverse" OCT pulses will not, in general, bear a simple relationship to those of the original pulses.

The overall optimization procedure for finding such inverse pulses was the same as shown in Figure 16. The main change was to the cost function to be minimized. In this case it can be written as

$$C = \int \left| m_{rx}\left(\Delta\omega_0\right) + m_{rx,orig}\left(\Delta\omega_0\right) \right| d\left(\Delta\omega_0\right) + \alpha \left| SNR - SNR_{orig} \right|.$$

This function contains two terms. The first term is minimized when the asymptotic magnetization produced by the new excitation pulse is the inverse of that produced by the original pulse, i.e., $m_{rx} = -m_{rx,orig}$ at all offset frequencies $\Delta\omega_0$. The second term is minimized when the two pulses produce the same SNR. The relative weight of these terms is controlled by the constant α, which we

usually set to 0.8. We assume that the original and inverse excitation pulses use the same refocusing cycle. This condition, of course, is necessary for phase cycling to be effective.

Figure 20 compares the phases of the original and inverse excitation pulses in two cases, center frequency of 250 kHz or 500 kHz. We see that there is no simple relationship between them, although a significant amount of anti-correlation is evident.

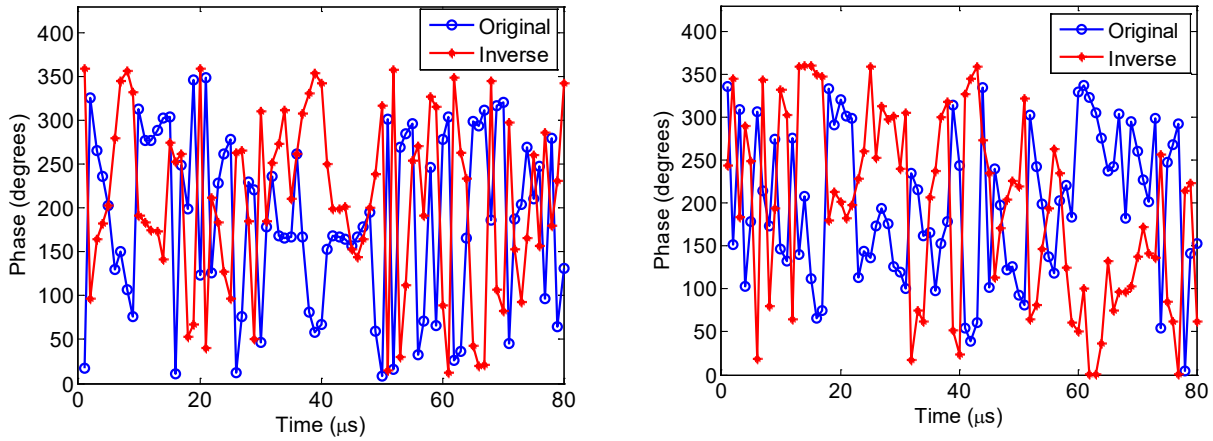

Figure 20: Pulse segment phases for original and inverse axis-matching excitation pulses at 250 KHz (left) and 500 kHz (right).

The asymptotic magnetization produced by original and inverse excitation pulses with the same refocusing cycle is shown in Figure 21. The results are almost perfect inverses of each other. This allows a two-part PAP cycle to be used during acquisition.

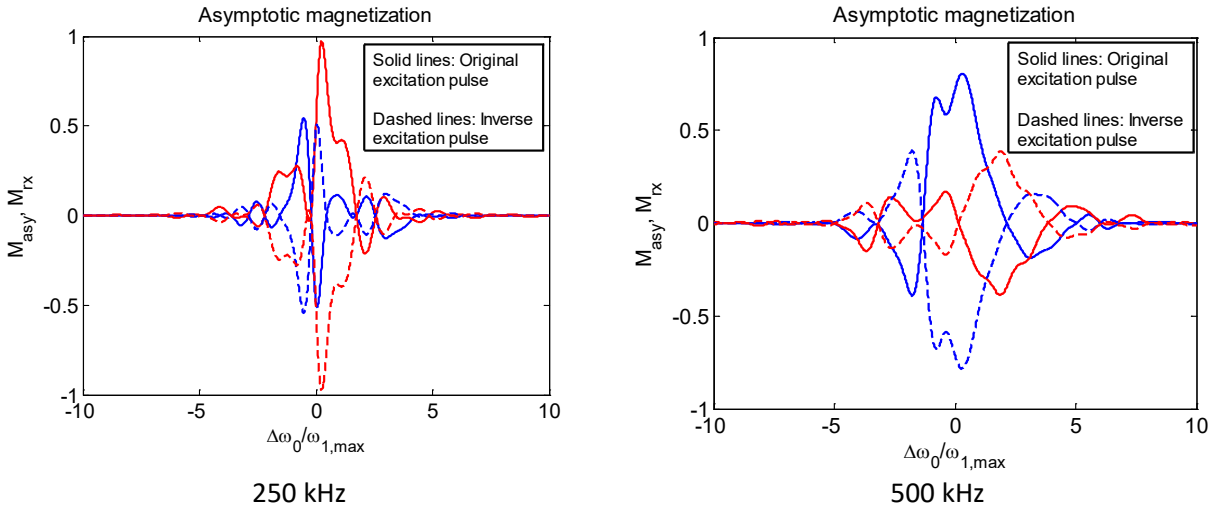

Figure 21: Simulated asymptotic magnetization for original and inverse axis-matching excitation pulses at 250 KHz (left) and 500 kHz (right). The same refocusing cycle was used with the original and inverse excitation pulses in each case.

Performance summary

The table below summarizes the simulated asymptotic SNR (in power units) of the OCT sequences that we have developed. Results at each nominal Larmor frequency have been normalized to the default

CPMG sequence (rectangular $\pi/2$, rectangular π pulses) at that frequency. The table shows the expected performance of the OCT sequences with and without PAP-type phase cycling using "inverse" excitation pulses. The asymptotic magnetizations produced by the original and inverse excitation pulses are not perfect inverses of each other, which results in a slight decrease in SNR with phase cycling. However, this effect is small.

Larmor frequency	Sequence type	Normalized SNR (no phase cycling)	Normalized SNR (phase cycled)
250 kHz	Rectangular	1.000	1.000
250 kHz	OCT	1.520	1.491
500 kHz	Rectangular	1.000	1.000
500 kHz	OCT	1.893	1.822

The OCT sequences produce substantially more SNR than the default CPMG with rectangular pulses, particularly as the Larmor frequency increases. This is mainly because the absolute receiver bandwidth increases, since its quality factor was kept constant.

In addition, it should be noted that the OCT sequences were optimized to have the same steady-state coil current and power consumption as the default CPMG. In practice, however, they consume somewhat more transmitter power, mainly because of coil current transients produced by phase transitions within the refocusing pulse. Fortunately, the phase varies smoothly within our optimized refocusing pulses, making the additional transients small. We calculated the resultant increase in transmitter power to be only 7.0% at 250 kHz, and 8.4% at 500 kHz.

Experimental results

We have performed some experiments with an un-tuned transmitter and probe to verify our results. This system has previously been used for a variety of low-frequency magnetic resonance experiments [5]. It consists of an H-bridge transmitter that drives an un-tuned solenoid coil containing the sample. Relevant circuit parameters at room temperature are shown in the table below. Note that the duplexer and receiver electronics have not been described since they were not used during these experiments.

Component	Role	Details
Probe	Un-tuned sample coil	Solenoid, ID = 2.7 cm, length = 8.4 cm, 42 turns, L = 15 µH
FDD6N20TM (Fairchild)	H-bridge MOSFET	$V_{DS,max}$ = 200 V, R_{on} = 0.6 Ω up to 3 A
FDD6N20TM (Fairchild)	MOSFET source-drain reverse protection diode	V_{on} = 0.8 – 0.9 V between 1 - 3 A
RCD snubber	Over-voltage protection	100 Ω || BAS321 diode, in series with 100 pF
IR2011 (International Rectifier)	Half-bridge driver	
BAS321 (NXP)	Cross-coupled diode pairs (x 2) to isolate transmitter from	R_s = 0.75 Ω, $V_{on} \approx$ 0.9 V

	receiver after turn-off (extender)	

Constant-amplitude RF pulses were fed into the transmitter from a Kea 2 spectrometer (Magritek). The transmitter contains circuitry that converts these low-level pulses (< 0 dBm) into logic-level drive signals for the MOSFETs in the H-bridge [1]. The resultant coil current was measured with a current probe and displayed on a digital oscilloscope. Typical results obtained with two rectangular input pulses at 250 kHz are shown in Figure 22. The waveform on the left displays transients at the beginning and the end of the second pulse. The former is well-fit by an exponential decay with time-constant $\tau \approx 6.0\ \mu s$, as shown on the figure. This result confirms the validity of the simple circuit model shown in Figure 1. This model predicts $\tau = L/\left(R_c + R_{s,on}\right)$, so we conclude that $R_c + R_{s,on} \approx 2.5\ \Omega$.

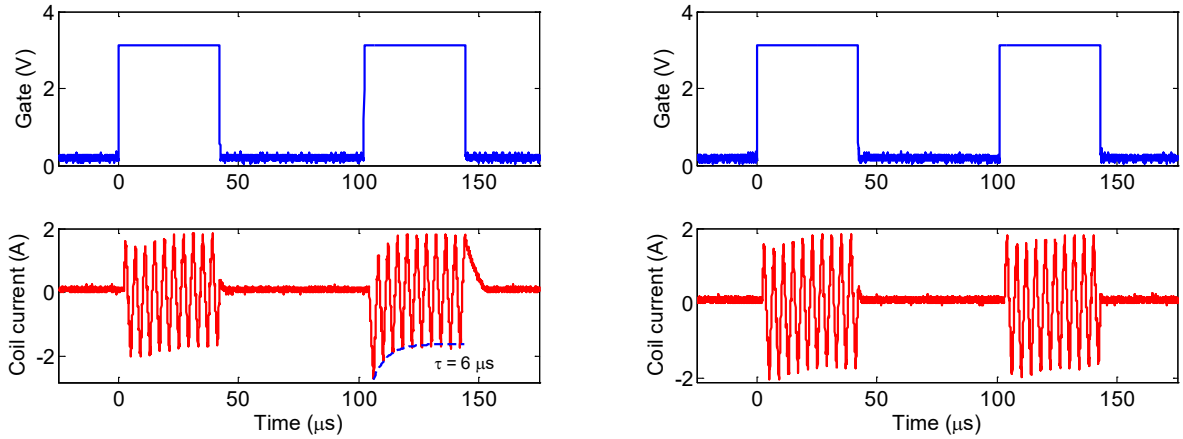

Figure 22: Measured coil currents produced by our un-tuned NMR transmitter at 250 kHz. The transmitter voltage was set to 30 V. The input consisted of two rectangular (constant amplitude and phase) RF pulses, each 40 µs long. The locations of these pulses are indicated by the "gate" pulses shown above each current waveform. The figure on the left shows that transients are produced both at the beginning and at the end of the second pulse. The former is well-fit by an exponential decay with a time constant τ = 6.0 µs. The figure on the right shows that the transients disappear when the delay between the two pulses is changed by 1 µs (one quarter of the RF period).

The expected value of $R_{s,on}$ is given by

$$R_{s,on} \approx 2R_{on,MOSFET} + R_{s,extender} \approx \left(1.2 + 0.8\right)\Omega = 2.0\ \Omega.$$

This prediction is in excellent agreement with our measurements if $R_c \approx 0.5\ \Omega$, which is a reasonable value for this coil at 250 kHz.

Interestingly, the turn-off transient is noticeably non-exponential – in fact, it is approximately linear. This is because we did not activate any "Q-switch" after the pulse turns off. Instead the inductor current had to discharge ("free-wheel") through the extender and MOSFET source-drain reverse diodes, as shown in Figure 23. However, the effective resistance of a diode varies inversely with the current through it, instead of remaining at a constant value $R_{s,off}$. This nonlinear I-V characteristic is responsible for the non-exponential transient visible in Figure 22.

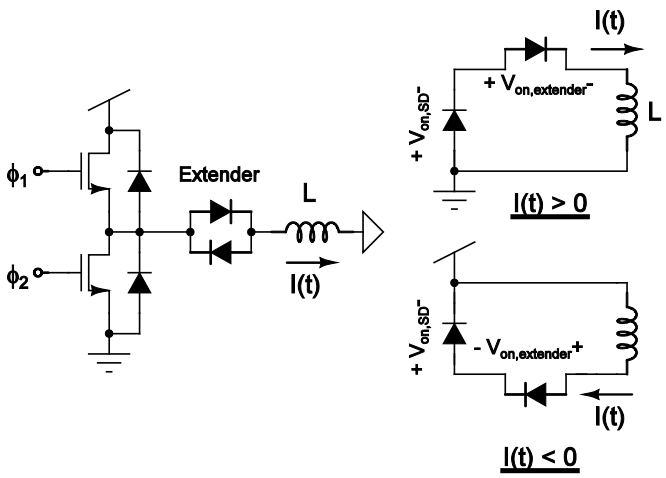

Figure 23: Simplified schematic of an un-tuned NMR transmitter and probe based on an H-bridge (left), and its equivalent circuit during pulse ring-down, i.e., after the transmitter has been switched off (right). We have split the differential transmitter and probe circuit into two parts down its axis of symmetry, i.e., the center of the coil, to simplify the analysis. Only one half-circuit is shown in the figure.

The free-wheel decay of inductor current through generic nonlinear resistors (defined by the I-V characteristic $I = kV^n$) has been analyzed in the literature [6]. One interesting finding was that the inductor current decays to zero in a *finite* time whenever $n > 1$, i.e., whenever the characteristic is nonlinear. This behavior is in contrast to an exponential decay, which takes an infinite amount of time to reach zero. An ideal diode can be viewed as the limiting case $n \to \infty$, so it is not surprising that the coil current in our measurements also goes to zero in a finite amount of time after the pulse switches off.

A simple model for the turn-off transient in this case can be made by assuming that the voltage across each diode remains constant at its "on" value. This results in a linear decrease in coil current, in good agreement with the measurements:

$$L\frac{dI}{dt} = V \approx -2\left(V_{on,SD} + V_{on,extender}\right) \Rightarrow I(t) = I(0) - 2\left(\frac{V_{on,SD} + V_{on,extender}}{L}\right)t.$$

The factor of two appears because of the other half of the H-bridge circuit (not shown in Figure 23). This equation predicts a pulse turn-off time, i.e., time taken to reach zero current, of

$$t_{off} = \frac{I(0)L}{2\left(V_{on,SD} + V_{on,extender}\right)}.$$

The measured slope of the coil current during turn-off is 0.21 A/µs, which corresponds to V_{on} = 3.15 V. This result is in good agreement with the predicted value, which is $V_{on} = 2\left(V_{on,SD} + V_{on,extender}\right) \approx 3.4\ \text{V}$. The measured turn-off time from $I(0)$ = 1.7 A is t_{off} = 8.1 µs.

Finally, the waveform on the right of Figure 22 shows that both transients disappear from the second pulse when the delay between the two pulses is increased by 1 µs, i.e., one quarter of an RF cycle.

Intermediate changes in the delay result in partial cancellation of the transients. Moreover, this behavior is periodic in the value of the delay, with a periodicity of half the RF cycle (2 μs). These results are in excellent agreement with our theoretical predictions.

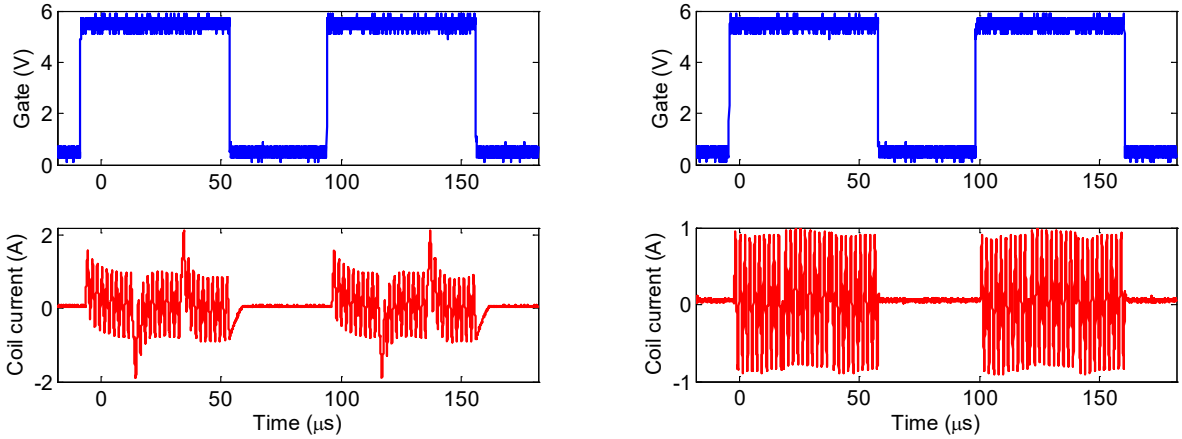

Figure 24: Measured coil currents produced by our un-tuned NMR transmitter at 500 kHz. The transmitter voltage was set to 30 V. The input consisted of two constant-amplitude RF pulses, each 60 μs long. Each pulse consisted of 3 segments of length 20 μs, with phases equal to 0, π, and 0, respectively. The locations of these pulses are indicated by the "gate" pulses shown above each current waveform. The figure on the left shows that transients are produced at the beginning and end of both pulses, as well as every time the phase changes within a pulse. The figure on the right shows that these transients disappear when the delay before the first pulse is changed by 0.5 μs (one quarter of the RF period).

We then extended our experiments to include phase-modulated pulses with multiple segments, as shown in Figure 24. These measurements were made at a frequency at 500 kHz. The plot on the left shows that large transients are produced at the beginning and end of each pulse, as well as every time the phase changes within a pulse. The plot on the right shows that these transients disappear when the delay before the first pulse is adjusted by 0.5 μs, i.e., one quarter of the RF period. Intermediate changes in the delay result in partial cancellation of the transients. Moreover, this behavior is periodic in the value of the delay, with a periodicity of half the RF cycle (1 μs). These results are in excellent agreement with our theoretical predictions.

A zoomed-in view of the first pulse (with transients cancelled) is shown in Figure 25. This figure shows that all phase transitions occur at zero-crossings of the coil current. This behavior is in agreement with our theoretical predictions for phase changes of $\pm\pi$ between segments.

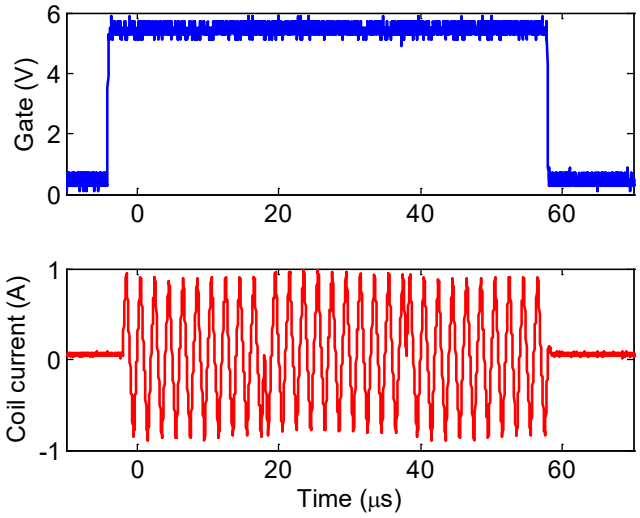

Figure 25: Zoomed in version of the right-hand plot in Figure 24, showing that all phase transitions occur at zero crossings of the coil current.

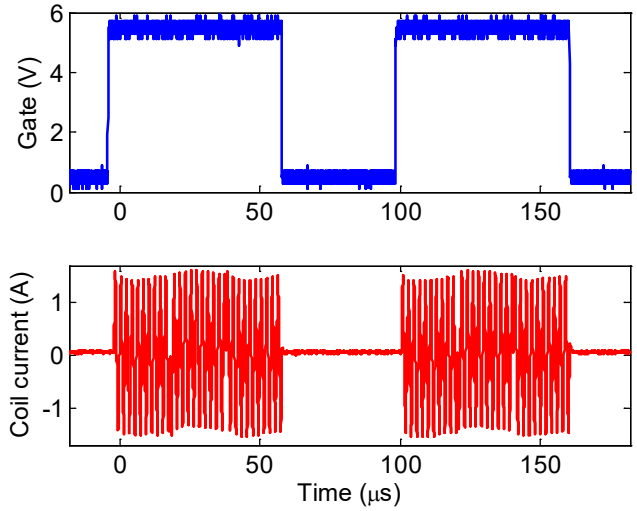

Figure 26: Measured coil currents produced by our un-tuned NMR transmitter at 500 kHz. The same pulse lengths and delays were used to draw this plot and the right-hand plot in Figure 24, except for the fact the transmitter voltage was increased from 30 V to 50 V.

Figure 26 shows the results of keeping all pulse lengths, delays, and other parameters fixed but increasing the transmitter voltage from 30 V to 50 V. We see that the transients are cancelled in both cases. This result shows that the cancellation conditions are (approximately) independent of the input voltage amplitude, as predicted by our switched-linear model.

Figure 27 extends these results by showing that it is possible to cancel transients at any input frequency. For instance, the set of data shown in this figure was measured at a frequency of 400 kHz. Only small adjustments to the pulse lengths and/or inter-pulse delays were required, as predicted by our theoretical analysis.

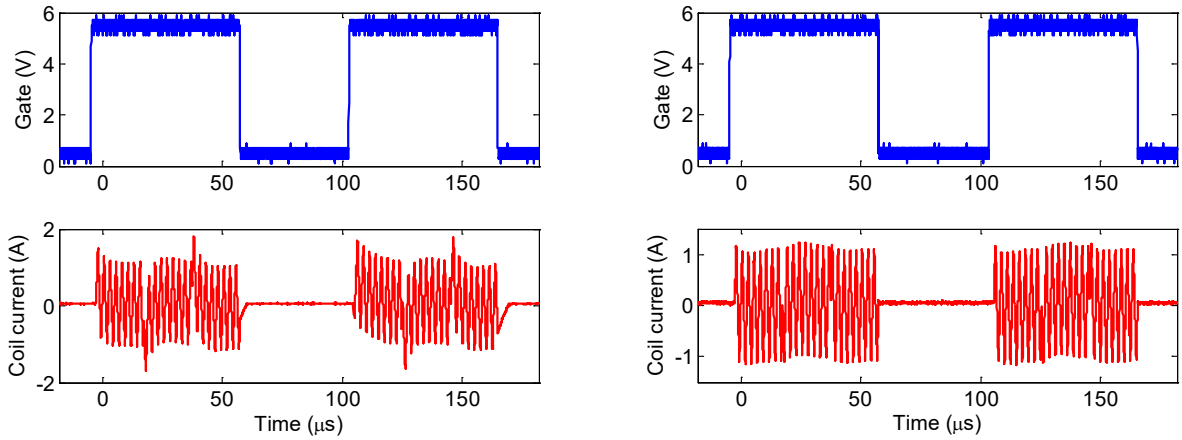

Figure 27: Measured coil currents produced by our un-tuned NMR transmitter at 400 kHz. The transmitter voltage was set to 30 V. The input consisted of two constant-amplitude RF pulses, each 60 μs long. Each pulse consisted of 3 segments of length 20 μs, with phases equal to 0, π, and 0, respectively. The locations of these pulses are indicated by the "gate" pulses shown above each current waveform. The figure on the left shows that transients are produced at the beginning and end of both pulses, as well as every time the phase changes within a pulse. The figure on the right shows that these transients disappear when the delay before the first pulse is increased by 0.2 μs, and the spacing between them by 1.2 μs.

Future work

We would like to run more experiments to further verify the conclusions of this report. We are currently developing a microcontroller-driven transmitter that is capable of precisely controlling the absolute phase of RF pulses. This system should allow us to eliminate current transients in un-tuned probes during typical NMR pulse sequences, such as the CPMG. We are also planning to combine this system with a tuned coil to evaluate the performance of OCT excitation and refocusing pulses designed for tuned NMR probes.

It would also be interesting to impose symmetry constraints on the OCT excitation and refocusing pulses. For example, it would simplify phase cycling and NMR data processing if they generated asymptotic magnetization that was real and symmetric about $\Delta\omega_0 = 0$, so that the resultant time-domain echoes were purely real. SPA refocusing pulses are known to satisfy these conditions in the absence of transmitter and receiver filtering, i.e., when probe dynamics can be ignored.

Acknowledgements

The author would like to thank Martin Hürlimann, Yi-Qiao Song, and Shin Utsuzawa for many useful discussions.

Bibliography

[1] S. Mandal, S. Utsuzawa and Y.-Q. Song, "Completely non-resonant NMR electronics," Schlumberger

internal report OFSR/RN/2011/196/SENSORPHYSICS/C, Cambridge, MA, 2011.

[2] S. Mandal and M. Hurlimann, "CPMG-type OCT sequences with longer refocusing pulses: Theory and experiment," Schlumberger internal report OFSR/RN/2013/072/SENSORPHYSICS/C, Cambridge, MA, 2013.

[3] V. D. M. Koroleva, S. Mandal, Y.-Q. Song and M. D. Hurlimann, "Broadband CPMG sequence with short composite refocusing pulses," *Journal of Magnetic Resonance,* vol. 230, pp. 64-75, 2013.

[4] M. D. Hurlimann and D. D. Griffin, "Spin Dynamics of Carr–Purcell–Meiboom–Gill-like Sequences in Grossly Inhomogeneous B0 and B1 Fields and Application to NMR Well-Logging," *Journal of Magnetic Resonance,* vol. 143, pp. 120 - 135, 2000.

[5] S. Mandal, S. Utsuzawa and Y.-Q. Song, "An extremely broadband low-frequency MR system," *Microporous and Mesoporous Materials,* 2013, in press.

[6] J. M. Diamond, "Varistor control of inductive transients," *IEEE Transactions on Circuits and Systems - I: Fundamental Theory and Applications,* vol. 39, no. 6, pp. 478 - 480, 1992.